A system for functional studies of the major virulence factor of malaria parasites

Jakob Cronshagen[1,2], Johannes Allweier[2,3], Joëlle Paolo Mesén-Ramírez[1†], Jan Stäcker[1], Anna Viktoria Vaaben[4], Gala Ramón-Zamorano[1,5], Isabel Naranjo-Prado[1], Max Graser[1], Patricia López-Barona[1], Susann Ofori[2], Pascal WTC Jansen[5], Joëlle Hornebeck[1], Florian Kieferle[2], Agnes Murk[2], Elicia Martin[4], Carolina Castro-Peña[1], Richárd Bártfai[5], Thomas Lavstsen[4], Iris Bruchhaus[2,6]*, Tobias Spielmann[1]*

[1]Pathogen section, Bernhard Nocht Institute for Tropical Medicine, Bernhard Nocht Str. 74, 20359 Hamburg.
[2]Interface section, Bernhard Nocht Institute for Tropical Medicine, Bernhard Nocht Str. 74, 20359 Hamburg.
[3]Biophysics, Research Center Borstel, Leibniz Lung Center, Parkallee 1-40, 23845 Borstel.
[4]Centre for translational Medicine & Parasitology, Department of Immunology and Microbiology, University of Copenhagen and Department of Infectious Diseases, Righospitalet, Copenhagen, Denmark.
[5]Department of Molecular Biology, Faculty of Science, Radboud University, 6525GA, Nijmegen, the Netherlands.
[6]Department of Biology, University of Hamburg, Ohnhorststr. 18, 22609 Hamburg, Germany.

† present address: Centre for Structural Systems Biology, Hamburg, Germany

*correspondence: spielmann@bnitm.de; bruchhaus@bnitm.de

Summary

PfEMP1 is a variable antigen displayed on erythrocytes infected with the malaria parasite *Plasmodium falciparum*. PfEMP1 mediates binding of the infected cell to the endothelium of blood vessels, a cause of severe malaria. Each parasite encodes ~60 different PfEMP1 variants but only one is expressed at a time. Switching between variants underlies immune evasion in the host and variant-specific severity of disease. PfEMP1 is difficult to study due to expression heterogeneity between parasites which also renders genetic modification approaches ineffective. Here, we used selection linked integration (SLI) to generate parasites all expressing the same PfEMP1 variant and genome edit the expressed locus. Moving this system from the reference strain 3D7 to IT4 resulted in PfEMP1 expressor parasites with effective receptor binding capacities. We also introduce a second version of SLI (SLI2) to introduce additional genome edits. Using these systems, we study PfEMP1 trafficking, generate cell lines binding to the most common endothelial receptors, survey the protein environment from functional PfEMP1 in the host cell and identify new proteins needed

for PfEMP1 mediated sequestration. These findings show the usefulness of the system to study the key virulence factor of malaria parasites.

Introduction

A key factor for the pathology of the human malaria parasite *Plasmodium falciparum* is its capacity to render the infected red blood cells (RBCs) adherent to the endothelium of blood vessels [1]. This cytoadhesion allows the parasite to escape spleen-mediated clearance of infected RBCs [2] but causes sequestration of infected RBCs in major organs, which can lead to severe, life-threatening complications including cerebral malaria [3].

Cytoadhesion is mediated by members of the *P. falciparum* erythrocyte membrane protein 1 (PfEMP1) family. PfEMP1s are 150 – 450 kDa single-pass transmembrane proteins inserted into the membrane of the infected RBC [4–7]. PfEMP1s are encoded by the two-exon *var* genes, with exon 1 encoding the variable extracellular part of PfEMP1 which has diversified to bind different host receptors such as CD36, ICAM-1, EPCR and CSA through its DBL and CIDR domains [4,7–13]. The *var* exon 2 encodes a conserved intracellular C-terminal part, the acidic terminal segment (ATS), which anchors the PfEMP1 underneath the RBC membrane in so-called knobs, parasite-induced elevations of the RBC membrane which contribute to efficient cytoadhesion of the infected RBC [14–16]. Each parasite genome contains ~45-90 *var* genes that differ in sequence within and between parasites, but confers each parasite a similar repertoire of human receptor-binding phenotypes [5,17–19]. Each parasite expresses only one *var* gene at a given time but can switch to a different *var* gene, resulting in antigenic variation [11,20,21]. While the diversity of *var* genes between isolates is high, the unique VAR2CSA PfEMP1 binding placental CSA - the cause of the detrimental sequestration leading to pregnancy malaria - is much more conserved between different isolates [9,10].

PfEMP1 is the major target for the protective acquired immune response [22] and *var* gene switching is important to escape immune recognition and a mechanism to establish long-term infection in the host [21–27]. Specific PfEMP1 variants are associated with pathology in the human host and with its immune status [9,13,28,29]. Understanding the binding properties of individual PfEMP1 variants, antibody recognition and switching is therefore critical to understand the pathology of malaria.

How PfEMP1 reaches its final destination at the host cell membrane is only partially understood. Exported parasite proteins are translocated by the PTEX complex into the host cell but it is not fully clear if this is also true for PfEMP1 [30–35]. Once in the host cell, PfEMP1 is most abundantly found at parasite-induced vesicular cisternae termed Maurer's clefts, and only a small fraction of all PfEMP1

molecules reach the host cell surface [16]. How PfEMP1 is transported within the host cell to reach the surface is unclear but a number of other exported proteins, e.g., SBP1 and PTP1-7 are needed for that process [36–39].

A key problem in studying PfEMP1 lies in the heterogenous *var* gene expression of the parasites in cell culture. This results in a mixed population of cells that have different antigenic and binding properties. Selective enrichment of binding phenotypes through elaborate panning of parasites against receptors or antibodies [40–43] or the utilization of parasite strains with more stable PfEMP1 expression, such as CS2 [42,44], have previously been used to circumvent this issue. A further problem is that specific PfEMP1s can be difficult to detect at the protein level. Antibodies against the conserved ATS do not distinguish between PfEMP1 variants and often cross-react with RBC spectrin [45]. Extracellular domain specific antibodies need to be generated for each newly studied PfEMP1 [7]. Furthermore, the large size hampers episomal expression and in some cases episomally expressed mini-PfEMP1s were used as a surrogate, e.g. to study PfEMP1 trafficking [30,34,46,47]. Finally, research questions needing genetic modification of PfEMP1s pose the problem that the modified locus is only expressed in some of the parasites.

Here we use selection linked integration (SLI) [48] to generate parasite lines that each predominantly express one specific PfEMP1 [49]. This permitted us to generate different parasite lines with binding specificities against all major binding receptors and parasites with modified PfEMP1s. We also introduce SLI version 2 (SLI2) to obtain a second genomic integration in parasites that already have a SLI-based alteration to express a specific tagged PfEMP1. We show that our approach can be used to study mutually exclusive expression of *var* genes, track the activated PfEMP1 via a small tag, study its trafficking, endothelial receptor binding, its proxiome in living parasites and identify novel proteins needed for PfEMP1-mediated cytoadhesion.

Results

Activation of specific PfEMP1 in the total cell population in 3D7 parasites

Using SLI [48], parasites were genetically modified to be resistant to G418 if expressing a targeted *var* gene (Fig. 1A), permitting selection of a population of parasites expressing the desired PfEMP1. In addition, the chosen PfEMP1 obtains a C-terminal 3xHA tag to specifically detect it (Fig. 1A). We first aimed to generate two different 3D7 parasite lines: in the first we targeted PF3D7_0809100, (*3D7var0809100*, the predominant *var* gene in our 3D7 wildtype (Fig. S1A)), and in the second PF3D7_1200600, the 3D7 VAR2CSA-encoding *var* gene. Cell lines with the expected genomic modification were obtained in both cases (3D7var0809100-HA^{endo} and 3D7var2csa-HA^{endo} parasites)

and the HA-tagged PfEMP1 was detected at the Maurer's clefts in the host cell (Fig. 1B, C), indicating that the cells in the culture expressed the desired PfEMP1 and that it could conveniently be detected via the epitope tag. qPCR showed predominant expression of the activated *var* genes (Fig. 1E, F). This was confirmed by RNA-Seq (Figure S1B, Table S2), which showed high read coverage across the desired *var* gene whereas transcripts of all other *var* genes were negligible (example in Figure S1C, Table S2). As PfEMP1 surface exposure is not typically detected using standard immunofluorescence assays, we conducted trypsin digestion assays with intact infected RBCs [50] which showed a protected fragment indicative of surface exposure of the HA-tagged PfEMP1 (Fig. 1D). When we lifted G418 pressure for 3 weeks, the dominance of the targeted PfEMP1 declined in favour of a more heterogenous *var* expression profile, indicating that switching to other *var*s was still possible in these parasites (Fig. 1E, F).

Previous work indicated that SLI to select parasites expressing a specific *var* gene can influence transcription of neighbouring genes that are oriented head-to-tail [49]. We did not observe activation of head-to-tail oriented *rifs* in our 3D7var0809100-HA^{endo} and 3D7var2csa-HA^{endo} SLI lines, as the corresponding *rifs* showed no or negligible transcription in RNA-Seq (Fig. S1D). To further look into co-activation, we used SLI to select for parasites expressing a *var* gene that shares a promotor region with a *rif* gene in a head-to-head orientation (PF3D7_0425800: cell line 3D7var0425800-HA^{endo}) (Fig. 1G, Fig. S1E). Correct integration of the plasmid into the genome and expression of the tagged PfEMP1 was confirmed (Fig. 1G). RNA-Seq showed predominant expression of the activated *var* gene (Fig. 1G) but also transcription of the neighbouring *rif* gene (Fig. S1F) with ~40% of all *rif* transcripts belonging to this *rif* gene (PF3D7_0425700) (Fig. S1G).

We also activated two *rif* genes (PF3D7_0425700: cell line 3D7rif0425700-HA^{endo} and PF3D7_1254800: cell line 3D7rif1254800-HA^{endo}) (Fig. S1H). The two resulting cell lines had the correct genomic modification and IFAs indicated expression of the HA-tagged RIFINs (Fig. S1H). qPCR showed that in both lines the activated *rif* gene was the most expressed (~65% and ~40% of *rif* transcripts) (Fig. S1I). While in the 3D7rif1254800-HA^{endo} parasite line the *var* expression profile looked similar to the 3D7 parent with predominant expression of *var* PF3D7_0809100 located on a different chromosome (Fig. S1I), activation of *3D7rif0425700* (which in contrast to *3D7rif1254800* has a *var* gene in head-to-head orientation) led to co-activation of the neighbouring *var* gene (PF3D7_0425800) (Fig. S1I). Overall, the data with activated *vars* and *rifs* suggests that neighbouring genes can be co-activated if in head-to-head orientation, likely due to a shared promotor region affected by the epigenetic changes resulting in the expression of the SLI-targeted *var* gene. While SLI-activation of *rif* genes also led to the dominant expression of the targeted *rif* gene, other *rif* genes

still took up a substantial proportion of all detected *rif* transcripts, speaking against a mutually exclusive expression in the manner seen with *var* genes.

Validation of a parasite line with impaired mutually exclusive *var* expression

Previous work described a 3D7 line expressing multiple *var* genes in single infected RBCs [51], likely due to a defective *var* regulation system, here designated $3D7^{MEED}$ (for "mutually exclusive expression defective"). We used SLI to obtain parasites expressing PF3D7_0425800 in the $3D7^{MEED}$ parasites ($3D7^{MEED}$var0425800-HA^{endo}) (Fig. 1H). In contrast to standard 3D7 with the same SLI modification to express *3D7var0425800*, $3D7^{MEED}$ showed elevated levels of transcription of multiple *var* genes in addition to the activated one, both by qPCR (Fig. S1E) and by RNA-Seq (Fig. 1H, I). Anti-HA IFAs showed that the $3D7^{MEED}$ parasite nevertheless expressed the activated PfEMP1 (all trophozoites were HA-positive in IFAs (n = 82 parasites from 4 independent experiments)) (Fig. 1H), indicating that individual parasites expressed multiple *var* genes. This line might therefore be an interesting tool to study mutually exclusive expression, silencing and switching mechanisms.

In an attempt to find changes that may cause the MEED phenotype, we compared all differentially expressed transcripts (161 down- and 93 up-regulated using a log2 fold change of >2 and Padjusted of < 0.05 as cut off) of the 3D7 vs $3D7^{MEED}$ parasites (Fig. 1J, Table S3). This confirmed the upregulation of most *var* genes in the $3D7^{MEED}$ parasites. Members of some other gene families encoding exported proteins and genes of other exported proteins were also upregulated. Many of these may be co-regulated with the *var*s, as for instance many of the upregulated *rif* gene loci are close to upregulated *var* loci (Table S3). However, a few genes encoding exported proteins were also downregulated. Concentrating on non-exported proteins to identify potential changes responsible for the MEED phenotype, we noticed that the transcripts encoding the ApiAP2 protein SIP2 [52] were down ~8 fold (pAdjusted ~0.025) (Fig. 1J, Table S3). SIP2 was previously shown to bind heterochromatin in subtelomeric and telomeric regions, including certain *var* promoters [52]. Its downregulation might result in changes to chromosome end biology influencing *var* silencing. The other potentially causal change was an upregulation of the non-coding RNA *ruf6* for which overexpression has been shown to impair monoallelic *var* gene expression [53]. While both *sip2* downregulation and *ruf6* upregulation are possible explanations for the relaxed silencing of *var* genes in the $3D7^{MEED}$ parasites, independent experiments are needed to confirm that any of these changes are reasons for the MEED phenotype.

Transport of PfEMP1 into the host cell

Next, we tested if SLI would permit to obtain parasites all expressing a modified PfEMP1 to track and study its transport. Limited overlap of PfEMP1 with PTEX components had raised the question

whether it is transported via PTEX or not [34,35]. While ablating PTEX function blocks PfEMP1 transport, indicating PTEX-dependent PfEMP1 transport [31,33], this may also be an indirect effect as inhibiting PTEX function also blocks the transport of other exported proteins essential for PfEMP1 transport. To directly assess PfEMP1 transport through PTEX, we used SLI to obtain parasites expressing VAR-0809100 (PF3D7_0809100) or VAR2CSA (PF3D7_1200600) and at the same time tagged them with mDHFR-3xHA (Fig 2A and Fig. S2). The folding of the mDHFR domain can be stabilised by addition of WR99210 (WR) which prevents transport through translocons requiring unfolding [54] and can be used to assess PTEX passage of soluble and transmembrane proteins in *P. falciparum* parasites [55,56] (Fig. 2A). Both mDHFR-fused PfEMP1s were efficiently exported to the Maurer's clefts but not blocked when WR was added (Fig. 2A). While this suggests that PfEMP1 might not be transported via PTEX, we previously noted that the length of the region between the transmembrane and mDHFR domain influences its blocking properties in exported transmembrane proteins [57] and it therefore cannot be fully excluded that this protein still uses PTEX for transport. To circumvent this problem, we exploited the property of proteins that – when fused to mDHFR – can be conditionally arrested in the PTEX translocon, preventing the passage of other exported proteins [57]. Blocking PTEX in that manner (using SBP1-mDHFR-GFP conditionally arrested in PTEX) prevented PfEMP1 transport (Fig. 2B), suggesting the need of PTEX function for PfEMP1 transport. However, similarly to previous work inactivating PTEX components [31,33], this does not exclude that PfEMP1 trafficking was prevented due to other exported proteins needed for PfEMP1 that were themselves prevented from export through PTEX. We therefore expressed the PTEX blocking construct later in the cycle (using the *crt* promoter) in an attempt to block PTEX passage only after the PfEMP1 trafficking proteins had already reached the host cell (Fig. 2C). Using this strategy, the early expressed PfEMP1-transport protein REX1 was still exported while a later-stage episomally expressed mScarlet-tagged KAHRP reporter could be blocked and was used to monitor clogging of PTEX after the parasite ring stage (Fig. 2C, D). We then inspected REX1 and PfEMP1 transport in the cells where the KAHRP-mScarlet reporter showed a late block of PTEX (Fig. 2D). REX1 was exported in most of the cells with a blocked KAHRP reporter, indicating that proteins needed for PfEMP1 trafficking were not hindered in reaching the host cell (Fig. 2D). However, PfEMP1, which is later expressed, showed accumulation around the parasite in the majority of cells (Fig. 2C). This indicated that clogging PTEX later in the cycle prevented PfEMP1 transport, supporting that PfEMP1 passes through PTEX. While we monitored only REX1, most PfEMP1-trafficking proteins show a similar early expression [34,58,59], indicating the effect may be direct, favouring the idea that PfEMP1 passes through PTEX. This would also mean that the mDHFR-based translocation block is not effective in the PfEMP1-mDHFR fusion construct.

SLI PfEMP1 expressor cell lines for binding studies using IT4 parasite strain

Next, we tested whether SLI PfEMP1-expressor parasites are useful for PfEMP1 binding studies. Initial experiments using 3D7 parasites with activated *var*s showed no or only minimal binding of infected RBCs to receptors (see below). We therefore moved to the FCR3/IT4 clone generally considered a cytoadhesion-competent parasite line [60,61] and used SLI to generate parasites expressing PfIT_040025500 (*IT4var66*), predicted to encode a CD36-binding PfEMP1 [62] with a similar domain composition to 3D7var080910, as well as PfIT_120006100 (*IT4var2csa*), encoding the IT4 VAR2CSA variant (Fig. 3A, B). Also, in IT4, SLI was effective to obtain parasites expressing the targeted *var*s and based on IFAs the HA-tagged PfEMP1 was expressed in the corresponding parasite lines (Fig. 3A, B). RNA-Seq showed predominant expression of the activated *var* genes (Fig. 3C, Table S2), and trypsin assays that the expressed PfEMP1 was presented on the RBC surface (Fig. 3D). For binding studies, we developed and validated a semi-automated pipeline to score the number of bound infected RBCs in binding assays to permit the unbiased and higher throughput scoring of bound infected RBCs and increase the number of fields that can be analysed per assay (Fig. S3). Both IT4 lines showed the expected receptor binding. The IT4var2csa-HA^{endo} infected RBCs bound both decorin-coated slides and endothelial cells expressing CSA (HBEC-5i) and binding was inhibited by soluble CSA (Fig. 3E, F). RBCs infected with IT4var66-HA^{endo} bound to CHO-CD36 but not CHO-GFP or CHO-ICAM-1 cells (Fig. 3G). In contrast, the 3D7 parasites expressing VAR2CSA (3D7var2csa-HA^{endo}) or 3D7var0809100 (3D7var0809100-HA^{endo}, predicted to bind CD36 [62]) did not or only poorly bind their respective receptors (Fig. 3E-G) despite the expressed PfEMP1 being detectable on the surface (Fig 1D). While the binding properties of PfEMP1 are difficult to compare between strains, VAR2CSA was chosen because it is well-conserved between isolates, permitting a comparison of binding efficiencies between 3D7 and IT4. Hence, these findings indicate that IT4 is a better cytoadhesion binder than the 3D7 used in our lab.

VAR2CSA is assumed to be the only PfEMP1 encoded in the genome that binds CSA. No binding to CSA was observed with the parental IT4 parasites (Fig. 3E, F) in agreement with the low levels of *var2csa* transcripts in these parasites (Fig. S1J). This indicated that SLI targeting *var2csa* selected this binding phenotype from undetectable levels. Overall, we conclude that SLI generated PfEMP1 expressor lines in IT4 can be used to study binding of specific PfEMP1 and that 3D7 - at least the version from our lab - is less suitable.

IT4 parasites with further binding properties

In order to extend the repertoire of cell lines to study PfEMP1 binding, we selected two known or suspected CD36- and ICAM-1-binders (PfIT_060021400; cell line IT4var01-HA^{endo} and

PfIT_120024500; cell line IT4var16-HA^{endo}) [63–65] and an EPCR-binder (PfIT_010005000: cell line IT4var19-HA^{endo}) [13]. Correct generation of the cell lines and expression of the desired *var* gene was confirmed (Fig. 4A-C). Trypsin assays showed surface exposure of the *IT4var01* and *IT4var16* but not *IT4var19* encoded PfEMP1 (Fig. 4D). Both, RBCs infected with IT4var01-HA^{endo} and IT4var16-HA^{endo} bound to CHO-CD36 and CHO-ICAM-1 cells but not GFP-expressing CHO cells, in agreement with the expected binding properties (Fig. 4E). IT4var16-HA^{endo} parasites showed a higher binding capacity to ICAM-1 than IT4var01-HA^{endo} parasites whereas IT4var01-HA^{endo} parasites showed proportionally more binding to CD36 than IT4var16-HA^{endo} parasites (Fig. 4E). In contrast, the IT4var19-HA^{endo} parasites showed no significant binding to EPCR, CD36 or ICAM-1 (Fig. 4F). However, after five rounds of panning against EPCR-expressing CHO cells, the panned IT4var19-HA^{endo} parasites exhibited significant binding to EPCR and to a lower degree to ICAM-1 (Fig. 4F) even though the *var* transcript profile was not noticeably altered compared to the unpanned IT4var19-HA^{endo} parasites and still showed predominant expression of *IT4var19* with similar overall *var* transcript levels (Fig. 4G; Fig. S1K). Trypsins assay of the panned parasites showed surface expression of IT4VAR19-HA (Fig. 4H), contrasting with the unpanned parasites (Fig. 4D). RNA-Seq indicated only few genes differently transcribed in the panned compared to the unpanned IT4var19-HA^{endo} parasites (Fig. 4I). Interestingly this included the two paralogs of *ptp3* that both were upregulated after panning. The single *ptp3* gene in 3D7 encodes a protein needed for PfEMP1 surface display in 3D7 [44], suggesting low *ptp3* expression as the reason for failure of the unpanned IT4var19-HA^{endo} parasites to bind. As the two *ptp3* loci in IT4 are more than ten genes apart, including 3 genes with comparable expression levels (to the *ptp3* genes) that were not differentially expressed in the panned parasites (PfIT_140083600, PfIT_140084100, PfIT_140084200), the initially low expression likely was not due to a genomic deletion but plastically altered transcription of *ptp3* genes.

In summary, we obtained parasites binding to the most common receptors although in the case of EPCR we had to pan the parasites and detected binding to ICAM-1 in addition to EPCR which was unexpected [40,43,66].

Additional genomic modification in SLI cell lines by using SLI2

To further exploit the SLI-generated PfEMP1 expressor parasites, we generated a second SLI plasmid system with different selection markers termed SLI2 to modify the genome of parasites already carrying a SLI modification (Fig. 5A). To test SLI2, we used the IT4var01-HA^{endo} line and applied SLI2 to disrupt PTP1 [44], a Maurer's clefts located PfEMP1 trafficking protein. Integration of the SLI2 plasmid into the correct genomic locus and perpetuation of the first genomic modification was confirmed by diagnostic PCR (Fig. 5B). Live cell imaging showed a GFP signal in the food vacuole

and faint diffused signal in the host cell, confirming successful inactivation of PTP1 (Fig. 5C). IFAs showed that in the PTP1-TGD parasites, SBP1 and PfEMP1 were found in many small foci in the host cell that exceeded the average number of ~ 15 Maurer's clefts typically found per infected RBC [67] (Fig. 5D). This phenotype resembled the previously reported Maurer's clefts phenotype of the PTP1 knock out in CS2 parasites [39]. PfEMP1 was still transported into the host cell in the PTP1 disruption parasites (Fig. 5D) but PfEMP1 was no longer surface exposed (Fig. 5E) and the parasites failed to bind to CD36 and ICAM-1 (Fig. 5F), indicating that the IT4var01-HA^{endo} parasites with the PTP1-TGD had lost their ability for cytoadhesion. While we did not detect the failure of PfEMP1 transport into the host cell, the binding phenotype agrees with previous work [39,44]. Hence, SLI2 permits the study of other proteins in SLI generated PfEMP1 expressor lines, for instance to study trafficking and binding of PfEMP1.

Proxiome of activated PfEMP1 using BioID

Next we assessed whether SLI could be used to obtain proxiomes (proximal proteins and interactors) of PfEMP1 in living parasites by generating parasites expressing a PfEMP1 fused with the promiscuous biotin ligase BirA* to carry out BioID [68]. For this we chose IT4var01 and generated three SLI cell lines with BirA* in different positions of that PfEMP1 (IT4var01-BirA*Pos1^{endo}, -2^{endo} and -3^{endo}) (Fig. 6A-D, Fig. S5). In position 1 BirA* was C-terminal to the ATS, in position 2 between transmembrane domain and ATS and in position 3 directly upstream of the transmembrane domain (Fig. 6A-D; note that *IT4var01-BirA*Pos3* lacked the intron (Data S1)). The resulting cell lines predominantly expressed the modified PfEMP1 (as judged by IFA and RNA-Seq), the PfEMP1 was on the surface and the infected RBCs showed the expected binding pattern (Fig. 6B-F). Parasites expressing the position 3 PfEMP1 construct showed less binding, suggesting partial impairment of placing BirA* into the extracellular part of PfEMP1. Nonetheless, overall the BirA* modified PfEMP1 were functional (Fig. 6F). BirA* in the PfEMP1 was active as judged by streptavidin blots which showed biotinylation with all 3 cell lines but not with the IT4 parent (Fig. 6G). Next, we carried out BioID experiments with these cell lines, analysing enrichment of biotinylated proteins over IT4 in two sequential protein extracts: first the proteins extractable by mild detergents (Fig. S5, Table S4) and the proteins requiring extraction with SDS to release more structurally connected proteins (Fig. 6H-J, Fig. S5, Table S4). In all experiments, the tagged PfEMP1 (but no other PfEMP1) was highly enriched due to self-biotinylation. Comparably few proteins were enriched in the mild detergent fraction (Fig. S5), but the SDS-fraction contained many proteins known to be important for PfEMP1 trafficking, including for instance SBP1, MAHRP1, REX1 and several PTPs (1, 2, 4, 5, 7), indicating efficient detection of PfEMP1 trafficking factors (Fig. 6H-J, Fig. S5). In addition, other exported proteins, were detected. This for instance included proteins of the MSRP6 complex found at the

Maurer's clefts which is involved in anchoring the clefts but has no role in PfEMP1 transport [67], several PHISTs [69] and exported proteins with unknown function here termed EMP1 interacting candidate 1-6 (EMPIC1-6) (Fig. 6H-J, Table S4).

Interestingly, the repertoire and relative enrichment of the proteins detected in the BioIDs with the three constructs was remarkably similar (Fig. 6H-J and Fig. S6A, Table S4), including position 3 where BirA* is located on the C-terminal side of the transmembrane domain. This supports the hypothesis that PfEMP1 is not transported as an integral membrane protein [30,70–72] as BirA* in the N-terminal part appears to have had access to biotinylate the same proteins as BirA* in the C-terminal part. While there was little evidence for topology-specific interactors, several of the detected PHISTs (PfIT_120058000, PfIT_040006400; PfIT_130076100) as well as GEXP10 and the less efficiently enriched PTEF are known to be RBC membrane localized [48,73–77], indicating that the proxiome also included hits from surface exposed PfEMP1. The hits obtained with the 3 PfEMP1 BirA*-fusion constructs were also more similar to each other than to a general Maurer's clefts proxiome or that of the MSRP6 Maurer's clefts binding domain [67], suggesting specificity for PfEMP1 (Fig. S6B). Further, hits from other structures than Maurer's clefts, such as the tether protein MAHRP2 [78] and the known [79,80] and likely [81] J-dot proteins HSP70x, GEXP18, and PHIST P2 (PfIT_120006500; Table S4) further supported that the PfEMP1 proxiome covered hits beyond its dominant location at the Maurer's clefts.

One notable difference between the hits of the 3 PfEMP1 BirA*-fusion constructs was that the position 1 construct detected 7 PHISTs, whereas the position 2 and 3 constructs only detected 3 and 2 PHISTs of which one was not detected with position 1 (Fig. 6H-J and Fig. S6A, Table S4). In addition, some of the PTPs (PTP1 and PTP7) appeared to be differentially enriched in the 3 positions. Finally, position 1 detected the largest number of enriched proteins, possibly because the larger distance from the transmembrane domain permitted more efficient labelling or because this part of the construct is in proximity to a larger number of proteins.

Taken together, these experiments detected most of the proteins previously implicated with PfEMP1 transport and surface display, indicating these proxiomes give a valid representation of proteins in contact with PfEMP1.

Identification of novel proteins needed for PfEMP1-mediated cytoadhesion

We selected several proteins from the PfEMP1 proxiomes (Fig. 6H-J, Table S4) that previously had not been connected with PfEMP1 transport and used SLI2 to generate full length tagged versions

(Fig. S7A) as well as disruptions (Fig. S7B) by targeting the corresponding genes in the IT4var01-BirA*Pos1^{endo} parasites to assess whether they could be needed for PfEMP1-mediated cytoadhesion. This included PfIT_020007200 that we had previously identified as a PEXEL negative exported protein (PNEP) exported to the host RBC periphery [48] and that was implicated in VAR2CSA translation and named *P. falciparum* translation enhancing factor (PTEF) [73]. We also included TryThrA (PfIT_080035200), a PNEP [82] that was a prominent hit in the BioIDs with all positions, including in the Triton fraction as well as EMPIC3 (PfIT_070007400), also a PNEP [82] detected with all 3 PfEMP1 BioID constructs with intermediate to high enrichment (Table S4; Fig. 7A). In addition, we included PeMP2 (PfIT_050006400), a member of the MSRP6 complex [67], not previously tested for its function in PfEMP1-mediated cytoadhesion.

Full length endogenously Ty1-tagged TryThrA, EMPIC3 and PeMP2 showed IFA patterns consistent with the reported localizations of these proteins in the host cell (Fig. S7A) [48,67,82]. For TryThrA-Ty^{endo} and EMPIC3-Ty^{endo} we observed cells where the Ty1 signal appeared as circles that likely corresponds to the Maurer's clefts periphery and only partially overlapped with the HA signal of PfEMP1 (Fig. S7A). This staining pattern is reminiscent of the subcompartmentalization of different proteins at the Maurer's clefts previously observed by superresolution microscopy [83].

Next, we examined the parasites wherein the selected candidates had been disrupted. While the SLI2-based disruptions of PTEF and PeMP2 did not result in loss of parasite binding to CD36 and ICAM-1, the TryThrA- and EMPIC3-TGDs resulted in markedly reduced binding (Fig. 7B), indicating TryThrA and EMPIC3 are novel proteins needed for cytoadhesion. Interestingly, the TryThrA-TGD parasites showed atypical localization of PfEMP1, SBP1, REX1 (dispersed signal in the host cell in addition to foci; disproportionally strong foci) but not KAHRP, pointing to a defect of the Maurer´s clefts or protein transport to these structures, while in the EMPIC3-TGD parasites PfEMP1, SBP1 and REX1 showed a localization typical for Maurer's clefts with clearly defined foci and absence of a dispersed pool (Fig. S7B).

In order to better define the phenotype in the TryThrA-TGD parasites, we transfected this and the EMPIC3-TGD parasite line with an episomal plasmid mediating expression of mCherry tagged SBP1, permitting analysis of live, unfixed parasites. As we had already used 4 selection markers to generate these parasites, we employed a plasmid encoding a mutated version of the lactate transporter FNT [84,85,86] that confers resistance to the chemical BH267.meta [87], to transfect these parasites and episomally express SBP1-mCherry (Fig. S8A). While in the EMPIC3-TGD parasites SBP1-mCherry was found in foci in the host cell typical for Maurer's clefts (Fig. S8B), the majority of the TryThrA-

TGD parasites showed an additional soluble pool of SBP1-mCherry in the host cell (Fig. S8C). Some TryThrA-TGD parasites also contained foci of increased intensity, suggesting enlarged or aggregated Maurer's clefts (Fig. S8C). As the IFAs showed a similar phenotype for REX1 and PfEMP1, the TryThrA-TGD parasites appear to have a defect in the localization of multiple Maurer's clefts proteins and possibly the morphology of the Maurer's clefts. These changes likely are responsible for the cytoadhesion defect in the TryThrA-TGD. In contrast no obvious changes explaining the binding phenotype were detected in the EMPIC3-TGD parasites.

To ensure the cytoadhesion defect was not due to unrelated changes that had occurred during generation of the TGDs, we sequenced the genome of the TryThrA and EMPIC3 TGD lines. No major changes compared to the cytoadherent IT4var01-BirA*Pos1^{endo} parent were detected that would explain the cytoadhesion defect (Table S5). Surface trypsin treatment assays showed that in both cases some PfEMP1 was still surface exposed (Fig. 7C), indicating that transport to the surface was either merely reduced or that an impairment of the correct presentation of PfEMP1 on the surface caused the binding defect. To ensure this was not due to limitations of the trypsin assay, we also disrupted PTP7, which also was a prominent hit in our BioIDs (Fig. 6I) and is a well-characterised PfEMP1 trafficking protein that results in loss of surface transport when disrupted [36]. We confirmed the cytoadhesion defect in the parasite with a disrupted PTP7 (Fig. 7B) and in contrast to the TryThrA and EMPIC3 TGD cell lines, trypsin assays indicated that there is no IT4VAR01-HA on the surface in that cell line (Fig. 7C).

In conclusion, we identified two novel proteins (TryThrA and EMPIC3) needed for PfEMP1 function. Given that many of the known PfEMP1 trafficking proteins were detected in the proxiomes and testing some of the others revealed more such proteins, we assume that the BioID experiments give a relevant representation of the protein environment of PfEMP1 and likely contain further proteins important for cytoadhesion.

Discussion

PfEMP1 is central for the virulence of *P. falciparum* parasites [3] and the main target of antibody mediated immunity in symptomatic malaria patients [22], but studying these important proteins is challenging. Using SLI we here generated cell lines predominantly expressing a PfEMP1 of choice and show that this facilitates the study of diverse aspects of PfEMP1 biology, including mutually exclusive expression, trafficking, interactome and receptor binding. A small epitope tag permits reliable tracking of the SLI-targeted PfEMP1, avoiding issues detecting specific variants or the ATS. In addition, we show that larger tags such as a mDHFR domain or BirA* can be added and used to

study transport or obtain the proxiome of functional PfEMP1 from living parasites. This also highlights positions in the PfEMP1 sequence where larger tags are tolerated, including in the external region, although the latter reduced the binding efficiency to some extent. Importantly, SLI ensures expression of the modified locus, which would be difficult with other approaches. We further introduce a second SLI system (SLI2) which permits a convenient further genomic modification while maintaining expression of the desired PfEMP1. This will also be of general usefulness to obtain double genome edited parasites.

The generated lines were capable to switch when G418 was lifted, indicating the system can be used to study switching and mutually exclusive expression of *var* genes. However, it should be noted that it is not known whether all mechanisms controlling mutually exclusive expression and switching remain intact in parasites with SLI-activated *var* genes.

Previous work indicated co-activation of genes in a head-to-tail position to the SLI-activated variant gene [49]. We here only found evidence of co-activation with the activated *var* with genes in a head-to-head orientation, suggesting this occurred due to a shared promoter, rather than a general relaxation of silenced chromatin around the active *var* gene. Similar head-to-head activation had been detected when parasites expressing specific *var* genes were enriched by panning [41]. However, it is unclear if this can be generalized and it is possible that different *var* loci respond differently. We also confirmed reduced mutually exclusive expression in a previously published 3D7 cell line [51] that we here termed $3D7^{MEED}$ and may be useful to study *var* silencing mechanisms.

PfEMP1-receptor binding and neutralising antibody mechanisms are increasingly being understood on a structural level and are relevant to understand malaria pathology and effectivity of the immune response in patients [88,89]. The straight forward capacity to generate cytoadherent parasite lines uniformly expressing a single PfEMP1 of interest opens up approaches to study receptor-binding as well as antibody-binding and inhibition using native as well as modified PfEMP1. The latter could be done by inserting point mutations, remove, exchange or alter domains e.g. by modifications directly in the original SLI plasmid or using CRISPR in the SLI-activated line.

An unexpected finding of this work was that IT4var19-expressing parasites bound ICAM-1 in addition to EPCR as this is considered a PfEMP1 that only binds EPCR [40,43,66], although some studies indicated that it may bind additional receptors [90,91]. Interestingly, selection for EPCR-binding was required to achieve avid EPCR binding of the *IT4var19* expressor line. While this binding selection did not change the *var* expression profile and IT4var19 remained the dominantly expressed PfEMP1,

we can not exclude this resulted in other changes that could have led to ICAM-1 binding. Selection for EPCR-binding was accompanied by higher expression of *ptp3* genes previously shown to affect PfEMP1 presentation and cytoadhesion [44], suggesting this as a reason why these parasites did not initially bind. As our findings indicate this was not due to a genome deletion, this raises the possibility of an additional layer controlling surface display through expression of PTP3 as an accessory factor by binding selection. Thus, the combination of uniform *var* expression and phenotype selection may enable detection of hitherto unrecognized PfEMP1 receptor phenotypes and phenomena controlling PfEMP1 surface display.

In the course of this work the binding phenotype of the *IT4var19* expressor line remained stable over many weeks without further panning. However, given that initial panning had been needed for this particular line, it might be advisable for future studies to monitor the binding phenotype if the line is used for experiments requiring extended periods of cultivation.

Previous work has indicated that mutants of the different proteins involved in PfEMP1 trafficking block its transport at different points on the way to the RBC surface, including at or before passing into the RBC [37–39,44]. Considering the results here and work on SBP1 disrupted parasites [67], none of these proteins seem to influence PfEMP1 before it reaches the Maurer's clefts. This aligns with the location of these proteins, which suggest that they function in the host cell. This would mean that the effect of PTEX inactivation on PfEMP1 transport [31,33] is likely direct, as the exported PfEMP1-trafficking proteins (if prevented from reaching the host cell due to the PTEX block) would not influence PfEMP1 before it reached the host cell. Together with the result from the stage-specific block of PTEX in this work, the currently most plausible scenario is that PfEMP1 is transported by PTEX after which other exported proteins are needed for transport to the surface and correct surface display. Why the mDHFR-fused PfEMP1 was not prevented in transport when WR was added is unclear, but may be due to the long region between the transmembrane domain and mDHFR [57] or due to the lack of GFP which might contribute to the effectivity of folding stabilized mDHFR to prevent translocation.

While our data indicates PfEMP1 uses PTEX to reach the host cell, this could be expected to have resulted in the identification of PTEX components in the PfEMP1 proxiomes, which was not the case. However, as BirA* must be unfolded to pass through PTEX, it likely is unable to biotinylate translocon components unless PfEMP1 is stalled during translocation. For this reason, a lack of PTEX components in the PfEMP1 proxiomes does not necessarily exclude passage through PTEX.

The PfEMP1 proxiome presented here comprised many of the known proteins required for PfEMP1-mediated cytoadhesion. There was a considerable overlap with the Maurer's clefts proxiome, where many of these proteins are localized. It, however, also included proteins experimentally confirmed to be located at other sites in the host cell, including the host cell membrane. Hence, despite the small number of PfEMP1 molecules displayed at the host cell surface [16], the proxiomes included hits from that site. A protein notably absent from our PfEMP1 proxiomes was the major knob component KAHRP [92–94]. While this was surprising in light of the original *in vitro* binding studies [95–97], a newer study was unable to detect an interaction of KAHRP with the ATS but found interaction with PHIST domains [98]. These findings match our proxiome data which, particularly with the position 1 construct, detected many PHIST proteins and suggests that PHISTs may be in more direct contact with the ATS than KAHRP. This also agrees with recent BioIDs with KAHRP as a bait that did not efficiently detect PfEMP1 whereas PTP4 as bait did [75].

We here report two new proteins needed for PfEMP1-mediated cytoadhesion. As we still detected some surface exposure of PfEMP1, the cytoadhesion defect was either due to reduced transport to the surface or due to incorrect surface display of PfEMP1. One of the identified proteins, TryThrA was in a recent study with 3D7 found to be dispensable for cytoadhesion [99]. It is possible that this discrepancy is due to the different *P. falciparum* strains used. In *P. berghei* IPIS3, which belongs to the same group of tryptophane-threonine-rich domain proteins, was recently found to be important for sequestration in rodent malaria [100]. Although mouse infecting malaria parasites do not possess PfEMP1, they do harbor orthologous machinery needed for sequestration, suggesting that virulence factor transport is evolutionary conserved even if the virulence factor is different [101]. This raises the possibility that tryptophan-threonine-rich domain proteins belong to the conserved core of this machinery, similar to SBP1 and MAHRP1 [101]. PTEF, selected because of its location at the host cell membrane [48] and previous linked to VAR2CSA translation [73], did not influence cytoadhesion of IT4VAR01.

The SLI system does have limitations for study of *var* and PfEMP1 biology. For example, if the targeted exon 2 region is too similar to that of other *var* genes, the SLI plasmid might insert into an unwanted *var* gene. This can be solved by providing a codon-changed exon 2 region in the SLI plasmid and shifting the targeting sequence upstream where there is high sequence variation. The feasibility of such an approach was shown here by generating the cell lines to insert BirA* into position 2 and 3 of IT4VAR01. Another limitation is that the discovery of PfEMP1-binding to unknown receptors may be difficult if, as seen with the IT4var19-HA^{endo} parasites, panning for receptor binding is required to select for that binding. However, as most PfEMP1 will bind CD36 or

EPCR, pre-selection on these receptors may enable studies of putative receptor-interactions. Alternatively, assuming PTP3 expression is causal and the only factor why the IT4var19-HA^{endo} parasites had to be panned, episomal expression of PTP3 could ameliorate this and possibly be used to generally enhance surface display and binding.

Acknowledgments

We thank Jacobus Pharmaceuticals for WR99210. DSM1 (MRA-1161) was obtained from MR4/BEI Resources, NIAID, NIH. This work was funded by the Joachim Herz Stiftung (Graduate School: Infection biology of tropical pathogens) (JC, TS, IB), the German Research Foundation grant BR 1744/17-1, SP1209/4-1 (IB, TS), the Jürgen Manchot Stiftung, Germany (JS), the Lundbeck Foundation grant R344-2020-934 (TL), the Independent Research Fund Denmark grant 9039-00285A (TL), Colciencias Scholarship, Columbia (INP), the Leibniz Collaborative Excellence grant K328/2020 (TS, RB), the European Research Council (ERC) under the European Union's Horizon 2020 research and innovation programme (grant agreement No. 101021493) (PLB, TS) and the Deutscher Akademischer Austauschdienst (DAAD) (CCP). The funders had no influence on the project.

Author contributions

Conceptualization: TS, IB, JC

Methodology: JC, JA, PMR, JS, AVV, INP, MG, PLB, SO, PWTCJ, JH, FK, AM, EM, CCP

Investigation: JC, TS, JA, GRZ

Visualization: JC, TS

Supervision: TS, IB, TL, RB

Writing—original draft: TS, JC

Writing—review & editing: JC, JA, PMR, JS, AVV, GRZ, INP, SO, PWTCJ, JH, FK, AM, EM, CCP, RB, TL, IB, TS

Declaration of interests

The authors declare no competing interests.

Data and materials availability

The RNA-Seq data have been deposited in NCBI's Gene Expression Omnibus [102] and are accessible through GEO Series accession number GSE267413, the whole genome sequencing data with the accession number GSE275671. The mass spectrometry proteomics data have been deposited to the

ProteomeXchange Consortium via the PRIDE [103] partner repository with the dataset identifier PXD052297.

Supplemental information titles and legends

Figures S1–S7

Tables S1 to S6

Table S1. qPCR results for the tested SLI lines

Table S2. RNA Seq and differential gene expression results for the tested SLI lines

Table S3. RNA Seq results comparing 3D7 and 3D7^{MEED} (each SLI modified to express PF3D7_0425800)

Table S4. Proteins enriched in the mass spectrometry results for the BioID cell lines and abbreviations used for proteins

Table S5. Whole genome sequencing comparison of Var01-EMPIC3-TGD and Var01-TryThrA-TGD parasites with the Var01 parent cell line (IT4var01-BirA*Pos1)

Table S6. Oligonucleotides used for diagnostic PCRs

Data S1 (Plasmids constructs)

Methods

Cloning of plasmid constructs

For genome integration constructs, homology regions encoding the C-terminus of target genes (for C-terminal tagging) or a region in the N-terminal part (for TGDs) were PCR amplified from 3D7 or IT4 gDNA (Monarch gDNA Purification Kit, NEB or QIAGEN DNA extraction kit) and cloned into pSLI [48] or pSLI2 using Gibson assembly [104] or T4 ligase. Plasmids, including the SLI2 plasmids and the FNT resistance plasmid for episomal expression of SBP1-mCherry, are shown in Data S1. For the Position 1 BirA* fusion plasmids, the targeting region followed by a 7xGGGS linker, a previously used sequence encoding BirA* [105] and a 3xHA-tag was cloned into pSLI. For position 2 and position 3 plasmids, the part of PfEMP1 encoded C-terminal to BirA* was synthesised with a different codon usage (GenScript) to prevent integration into the genome in that region and was cloned together with the targeting region (Position 2: until amino acid 2415; Position 3: until amino acid 2376), the region encoding BirA* flanked by short linkers and a 3xHA-tag into pSLI. For the episomal early stage blocking construct SBP1-mDHFR-GFP was cloned into pARL2 containing a *mal7* promotor [58]. For

the tagging of PfEMP1 with mDHFR, homology regions encoding the C-terminus of the target *var* genes were cloned into pSLI with a mDHFR domain between the targeting region and a 3xHA-tag. To ensure there were no undesired mutations, all cloned inserts were sequenced by Sanger sequencing (Microsynth).

Parasite culture

P. falciparum parasites (3D7 [106] and IT4 [107] were cultured using standard procedures [108]. The parasites were maintained in RPMI1640 supplemented with 0.5% Albumax (Life Technologies) and human 0+ erythrocytes (University Medical Center Hamburg-Eppendorf (UKE), Germany) at a haematocrit of 5% at 37°C under an atmosphere consisting of 1% O_2, 5% CO_2, and 94% N_2.

Transfection, SLI and confirmation of correct genome integration

Late schizont stage parasites were purified using percoll as described [109], using 60% percoll for 3D7 and 64 % for IT4 parasites. Fifty µg of purified plasmid DNA (Qiagen) were transfected using the Amaxa system (Lonza Nucleofector II AAD-1001N, program U-033) following previously described protocols [110]. Transfectants were selected with either 4 nM WR99210 (Jacobus Pharmaceuticals; pSLI) or 2 µg/µl blasticidin S (Life Technologies; pSLI2). SLI for selection of parasites with the plasmid integrated into the genome was done as described [48] by adding 400 µg/mL G418 (ThermoFisher; pSLI) or 0.9 µM DSM1 (Sigma Aldrich; pSLI2) to the culture. After the parasitaemia recovered under drug selection, genomic DNA was isolated and correct genomic integration of the plasmid in the knock-in parasites was verified by PCR as described [48]. For transfection of the plasmid harboring the mutated gene encoding PfFNT (amino acid change G 107 S) [86] BH267.meta [87] was used at 5 µM until parasites appeared after which the concentration of drug was dropped to 2.5 µM to maintain the culture.

Immunofluorescence and streptavidin-fluorescence assay

IFAs were performed as described [111]. Briefly, pelleted parasites (2000g for 5 min) were washed with 1x PBS and applied at a haematocrit of 1-2.5% to 10-well glass slides, air-dried and fixed in acetone for 30 min. Wells were rehydrated with 1x PBS, then washed 5 times with 1x PBS. Antibodies were applied in 1x PBS containing 3% BSA. Primary antibodies were rat anti-HA (Roche), 1:2000; rabbit anti-HA (Cell Signaling Technology), 1:1000; rabbit anti-SBP1-C [57], 1:2500; rabbit anti-KAHRP (kind gift of Prof. Brian Cooke), 1:500; mouse anti-EXP2 (European Malaria Reagent Repository) used 1:500; rabbit anti-REX1 [57], 1:10000; mouse anti-Ty1 (Sigma Aldrich), 1:20000; rat anti-RFP (Chromotek), 1:1000; mouse anti-GFP (Roche) used 1:1000 and rabbit anti-GFP (Thermo), 1:1000. For secondary antibodies donkey anti-rabbit conjugated with Alexa Fluor-488, or -594, goat anti-

rabbit conjugated with Alexa-647, goat anti-mouse conjugated with Alexa Fluor-488, goat anti-rat conjugated with Alexa Fluor-488, or -594 (Invitrogen) were used (all 1:2000). Secondary antibodies were applied together with 4',6'-diamidine-2'-phenylindole dihydrochloride (DAPI) (1µg/ml) or Hoechst (50ng/ml; Cayman) (as indicated in the figure legends) for staining of parasite nuclei. For the Streptavidin-fluorescence assay, streptavidin coupled to Alexa Fluor 594 (Invitrogen) was added (1:2000) together with the secondary antibody. Slides were mounted with Dako (Sigma Aldrich) and covered with a cover slip.

Fluorescence microscopy imaging

Live or fixed parasites were imaged with a Zeiss AxioImager M1 or M2 equipped with a Hamamatsu Orca C4742-95 camera using a 100×/1.4-numerical or a 63×/1.4-numerical aperture lens. AxioVision software (version 4.7) was employed to capture the images. Live cell imaging of parasites expressing fluorescent proteins was performed as previously described [112]. To stain the parasites DNA, parasites were incubated with either 1 µg/µl of DAPI (Roche) or 50 ng/ml Hoechst 33342 (as indicated in the figure legends) in parasite medium for 10 min at 37°C. Images were processed in Corel Photo-Paint (version 2021) and arranged in Corel Draw (version 2021).

Trypsin assay to assess PfEMP1 surface exposure

Parasite cultures with 5-10% parasitaemia were synchronised for rings using sorbitol [113] and then grown for 12 h at 37°C. The resulting trophozoite stage parasites were isolated with a percoll gradient as described [114] for 3D7 cell lines. For IT4 parasites, an adjusted gradient with 80%, 64% and 40% percoll was used. The purified infected erythrocytes were washed and split into two samples. One sample was incubated with 50 µg/ml TPCK-treated Trypsin (Merck) in 1x PBS at 37°C for 30 min while the other sample (control) was incubated in 1x PBS alone. Thereafter trypsin inhibitor from soybean (Sigma Aldrich) was added (1 mg/ml final concentration) and the samples were incubated on ice for 15 min. The cells were washed in 1 x PBS then lysed in 100 µl lysis buffer (4% SDS, 0.5% Triton X-100 in 0.5x PBS), containing 1 mg/ml trypsin inhibitor, 1 mM PMFS (Thermo Fischer) and 1x protein inhibitor cocktail (Roche). Extracts were immediately subjected to SDS PAGE or frozen at -20°C until needed.

Binding assays

For binding assays, Chinese Hamster Ovary (CHO-745 or CHO-K1) cells that express CD36, ICAM-1, GFP [65] or EPCR (in CHO-K1) [115], or human brain endothelial cells HBEC-5i cells (American Type Culture Collection (ATCC), Manassas, VA, USA; no. CRL-3245) were seeded two (1 x 10^5 cells/ml) or three (2 x 10^5 cells/ml) days before the binding assay into a 24-well plate containing coverslips

(0.5 ml/well). For binding assays against decorin (chondroitin sulfate proteoglycan from bovine articular cartilage previously used for VAR2CSA binding [116]), the coverslips in 24-well plates were incubated overnight at 4°C with decorin solution (5 µg/ml in PBS), thereafter washed with 1x PBS, blocked with 1 % BSA in 1x PBS for 2 h and washed with 1x PBS twice [117]. Knobby parasites of the tested cell lines were enriched using 1 % gelatine in glucose-free RPMI (16,4 g/l RPMI-HEPES (Applichem), 0.05 g/l hypoxanthine (Sigma Aldrich), 30 ml/l $NaHCO_3$ (7.5 %) (Merck) and 250 µl/l gentamycin (Ratiopharm) in H_2O, pH 7.2) as described [118]. After washing in binding medium (16,4 g/l RPMI-HEPES and 20 g/l glucose in H_2O, pH 7.2), number of erythrocytes/ml (Neubauer counting chamber) and % infected erythrocytes (Giemsa smears) were determined and the suspension adjusted to $2x10^6$ infected erythrocytes/ml in binding medium. The wells with the CHO or HBEC-5i cells were incubated with binding medium for 30 min before the parasite suspension was added to the wells (500 µl/well). Per experiment, three wells per parasite cell line and receptor were used. In the binding assays with decorin and HBEC-5i, the parasites suspension was split and either incubated with soluble CSA (100 µg/ml) or soluble BSA (100 µg/ml) (control) for 30 min at 37°C before adding the infected erythrocytes to the wells. The plates were then incubated for 60 min at 37°C for binding, with careful shaking every 15 min. The coverslips were washed 6 times by carefully dunking them into binding medium and blotting excess medium on paper after every dunk. The coverslips were then laid face-down parallel to the table in a washing plate that was angled at 45° (with the face-side hanging free in the binding medium) and incubated for 30 min at room temperature. Immediately after, the coverslips were fixed in 1% glutaraldehyde in 1x PBS for 30 min and stained with filtered 10% Giemsa (Merck) in 1x PBS for 15 min. The stained coverslips were washed in water and glued with CV-Mount (Leica) face-down onto glass slides. Five images per coverslip (per experiment 15 images per parasite line and condition) were captured with a Thermo Fisher EVOS xl (75 % light intensity at 40x magnification).

Automated counting of binding assays

The evaluation of images of binding assays was automated using Ilastik v1.3.3post3 [119] and CellProfiler v4.2.1 [120] (Fig. S3). First the images of the binding assays were processed with a trained Ilastik model for the segmentation of the foreground (infected erythrocytes) and background (CHO/HBEC-5i cells and plastic). For the training, the pixel classification module was manually trained with 20 microscopy images representing different shapes of infected erythrocytes, backgrounds, and artefacts. All the color/intensity, edge and texture features were enabled for training. The resulting processed images were exported as probability images with pixel intensities from 0.0 – 1.0 for the probability of a foreground pixel (regression values; 1.0 = 100 % probability for foreground pixel). Ilastik pre-processed images were then fed to a CellProfiler pipeline (Fig. S3)

using the "IdentifyPrimaryObjects" module to identify and count roundish objects with a diameter of 15 – 35 pixel units. Robust background thresholding and de-clumping by shape was selected. Number of counted infected erythrocytes scored per image was given out as a spreadsheet. To show the reliability of the automated pipeline in comparison to the manual scoring statistical tests between the two methods were conducted as shown in Fig. S3.

RNA-Seq and qPCR analysis

Synchronous ring-stage parasites with a parasitemia of 3 - 5%, from 10 ml of culture were pelleted at 800 g and dissolved in 5 pellet volumes of Trizol (Thermo Fischer), thoroughly mixed, incubated for 5 min at 37°C and immediately stored at -80°C until RNA isolation. To purify the RNA, the Trizol sample was thawed, 1/5 volume of chloroform added, thoroughly mixing and centrifuged at 16000 g for 30 min at 4°C. The resulting clear supernatant was transferred to a new tube and processed using the Qiagen miRNeasy Mini Kit according to the manufacturer's instructions. RNA integrity was assessed using the Agilent 2100® bioanalyzer system with the RNA 6000 Pico Kit. All samples had a RIN > 8, our cutoff for inclusion.

Ribosomal RNA was removed using QIAseq FastSelect RNA Removal Kit. Libraries were prepared with the QIASeq Stranded mRNA Library Kit and sequenced on an Illumina NextSeq 550 system with NextSeq 500/550 Mid Output Kit v2.5 (150 cycles). Raw reads were mapped with hisat2 (version 2.2.1) to the respective reference genomes sourced from PlasmoDB [121] (IT4: Release 58; 3D7: Release 62). Mapped reads were sorted and indexed with samtools (version 1.17). Reads mapped to genomic features were counted using featureCounts (version 2.0.4). For *var* genes, only reads mapping to exon 1 were considered, for *rifs*, reads to the entire coding region were included. The data have been deposited in NCBI's Gene Expression Omnibus [102] and are accessible through GEO Series accession number GSE267413. Python3 (version 3.11.4) and bioinfokit (version 2.1.2) were used to normalize the reads to transcripts per million (TPM) as well as to create the coverage plots with matplotlib (version 3.7.2). Volcano plot was done in GraphPad Prism. Differential gene expression analysis for panned against unpanned parasites was performed in R with the DESeq2 (version 1.42.0) package.

Quantification of *var* and *rif* transcript levels were measured relative to internal control gene seryl-tRNA synthetase by real-time quantitative PCR using primers specific to each 3D7 *var* or *rif* gene as previously described [122].

Assays to analyse PfEMP1 transport into the host cell

Assays assessing the transport of PfEMP1 fused directly to mDHFR [54], were done as described [56] with some modifications: schizont stages of the corresponding lines were purified with Percoll and

allowed to invade for 8 hours, followed by synchronisation with 5% sorbitol [113] to obtain ring stages with an age of 0-8 hours post invasion, the culture split into one with 4 nM WR and one without (control) and grown for 24 h before analysis by IFA. For co-blocking assays [57], where transport through PTEX was assessed indirectly by conditionally clogging it with another exported protein fused to mDHFR, the parasite cultures were synchronized using percoll to obtain schizonts as described [109] and grown for 24 h in the presence or absence of 4 nM WR followed by analysis of export by live cell imaging or IFA. For the late stage PTEX block the pARL2-SBP1-mDHFR-GFP-2A-KAHRP-mScarlet plasmid was utilized [57].

BioID, mass spectrometry and data analysis

For proximity biotinylation, biotin (50 µM final) was added to asynchronous parasites expressing the BirA*-PfEMP1 fusion constructs as well as to IT4 parent parasites (5% parasitemia, 150 ml per condition and experiment) and cultured for 24 h with one exchange of medium with fresh biotin after 12 h. Thereafter, the parasites were washed twice with DPBS before they were subjected to saponin lysis (0.03% saponin in DPBS) on ice for 10 min, followed by five washes in DPBS before lysis in 2 ml lysis buffer (50 nM Tris-HCL pH7.5, 500 mM NaCl, 1% Triton-X-100, 1 mM DTT, 1 mM PMSF and 1x protein inhibitor cocktail) and storage at -80°C. For isolation of proteins, the samples were thawed and frozen two times before centrifugation at 16,000 g for 10 min. The supernatant (Triton-extract) was saved and the pellet frozen, thawed and once more extracted using 4% SDS in 50 nM Tris-HCl pH7.5, 500 mM NaCl, 1% Triton-X-100, 1 mM DTT (SDS-extract). The SDS extract was transferred to a fresh tube and cleared by centrifugation at 16’000 g for 10 min. For the purification of biotinylated proteins, both extracts (Triton and SDS) were diluted 2:1 in 50 nM Tris-HCl and incubated with 50 µl Streptavidin Sepharose (GE Healthcare) overnight at 4°C while rotating. The beads were washed twice in lysis buffer, once in H_2O, twice in Tris-HCl pH 7.5 and three times in 100 nM Triethylammonium bicarbonate buffer (Sigma Aldrich). The proteins on the beads were digested as described [123]. Briefly, the beads were treated with 50 µl elution buffer (2 M Urea in 100 mM Tris pH 7.5 containing 10 mM DTT) at room temperature, shaking for 20 min. Subsequently, iodoacetamide (IAA) was added to a final concentration of 50 mM and the samples were further incubated in the dark, shaking for 10 min. The proteins were then treated with 0.25 µg Trypsin/LysC (Promega, #V5072), while shaking at room temperature. After two hours, the supernatants containing eluted proteins were collected and the beads were immersed with an extra 50 µl of elution buffer for 5 min at room temperature. The supernatant was pooled with the previous elution and the final 100 µl of eluted proteins were supplemented with 0.1 µg of Trypsin/LysC and treated overnight while shaking at room temperature. The protein samples were then desalted on Stagetips using C18 membranes [124] and eluted in 80% acetonitrile, 0.1% Formic acid.

The acetonitrile was evaporated in a SpeedVac and the concentrated sample was then reconstituted to a final volume of 12 µl with 0.1% Formic acid. To analyse the sample by mass spectrometry, 5 µl of sample was analysed during a 60 min on an Easy-nLC 1000 (Thermo Fisher Scientific) with a 30 cm C18-reverse phase column coupled on-line to an Orbitrap Exploris 480 mass spectrometer (Thermo Fisher Scientific). Data was acquired in top20 mode with a dynamic exlclusion of 45 sec.
Raw mass spectrometry data were processed using MaxQuant [125] (version 1.6.6.0). Parameters were set to default except for the following: Deamidation (NQ) was added as a variable modification together with oxidation (M) and acetyl (N-term). Match-between-runs and re-quantify options were enabled with default parameters and iBAQ values were calculated. Mass spectra were compared to peptide masses from the *Plasmodium falciparum* IT4 annotated proteome (PlasmoDB v64). The "proteinGroups" file from MaxQuant output was analysed using the Perseus software package [126] (version 1.4.0.20). The data were filtered against peptides assigned as "only identified by site", "reverse" and/or "potential contaminant" hits in the datasets. IBAQ values were transformed to log_2 values and missing values were imputed following a normal distribution. Data obtained from Triton-extraction and SDS-extraction were analysed separately. Significant outliers were identified at each position by using the two-sided Benjamini-Hochberg test with an FDR cut-off of 0.05. The mass spectrometry proteomics data have been deposited to the ProteomeXchange Consortium via the PRIDE [103] partner repository with the dataset identifier PXD052297.

Western Blot analysis

Western blots were conducted as described [114]. In brief, preparation of extracts from the BioID experiments or the trypsin cleavage assays were centrifuged at 16'000 g and the supernatant was mixed with 4x Laemmli sample buffer. Samples were incubated for 10 min at 90°C before they were applied to 10% polyacrylamide gels for sodium dodecyl sulfate polyacrylamide gel electrophoresis. The proteins separated on the gels were transferred to nitrocellulose membranes (Amershan Protan membranes, GE Healthcare) using transfer buffer (0.192 M Glycine, 0.1% SDS, 25 mM Tris and 20% methanol in H_2O). For the detection of proteins by antibodies, membranes were blocked in 5% skim milk (Roth) in 1x TBS (50mM Tris and 150 mM NaCl in H_2O) for 2 h at room temperature, washed three times with 1x TBS with 1% Tween and incubated in 1x TBS with 3% skim milk with the first antibody rolling overnight at 4°C. First antibodies were rat anti-HA (Roche) (1:1000); rabbit anti-SBP1-N (1:4000) [57] or rabbit anti-aldolase (1:4000) [57]. Secondary antibodies were horseradish peroxidase (HRP)-conjugated anti-rat (Dianova) (1:2000) or HRP-conjugated anti-rabbit (Dianova) (1:2000) and were applied in 1x TBS with 3% skim milk and incubated rolling for 2 h at room temperature. For the detection of biotinylated proteins, HRP-conjugated streptavidin was used in 5% BSA in 1x TBS as described [127] and incubated by rolling overnight at 4°C. After secondary antibody

or HRP-conjugated streptavidin incubation, the membrane was washed 3 times in 1x TBS with 1% Tween, then 5 ml ECL solution A (0.025% luminol (Sigma Aldrich) in 0.1 M Tris-HCL in H_2O, pH 8.6) was mixed with 500 µl ECL solution B (6,7 mM p-Coumaric acid in DMSO) and 1.5 µl H_2O_2 and applied to the membrane before the ECL signal was detected with a ChemiDoc XRS imaging system (Bio-Rad).

Whole genome sequencing and analysis

Genome sequencing was done essentially as described [128]. The NEBMonarch Genomic DNA Purification Kit was used to prepare genomic DNA from 50 ml cultures of the TryThrA and EMPIC3 TGD parasites (both generated in the IT4var1-BirA*Pos1^{endo} background) and from the parent (IT4var1-BirA*Pos1^{endo}). BGI TECH SOLUTIONS (Hong Kong) carried out DNBSEQ PE100 sequencing and bioinformatic analysis. This included calling of SNP, InDel, SV, and CNV compared to IT4 reference. The data was deposited at GEO (Accession number GSE275671) which also includes technical details on sample preparation and filtering. All SNPs leading to a stop or potential splice mistake, all INDELs leading to frame shifts, all SVs and CNVs indicating gene or partial gene loss in the Var01-TGD parasites that were not present in the parent (IT4-Var01 parasites) were manually assessed by inspecting the reads in that region. Only changes affecting exported proteins were considered and were manually re-assessed in all 3 lines by analysing the individual reads. In addition, known PfEMP1 trafficking genes were manually checked for differences.

Quantification, statistical analysis and figure construction

P values are indicated in the figure and $P<0.05$ was considered as significant. All error bars shown are standard deviations. Statistical significance was determined by unpaired t-test. A ratio-paired t-test was used for the comparison between the individual images of the binding assays evaluated by manual scoring and the automated pipeline. Statistical analysis was done in GraphPad Prism (version 9). Intraclass correlation coefficient (ICC) was calculated using excel (Microsoft); Two-factor ANOVA without replication was applied; ICC was calculated with the variations of the ANOVA; $ICC = MS_{Row}-MS_{Error}/MS_{Row}+df_{Column}xMS_{Error}+(df_{Column}+1)x(MS_{Column}-MS_{Error})/(df_{Row}+1)$. Graphs were done in GraphPad (version 9) and transferred to CorelDraw (version 2021) with adjustments to style without altering the data. Corel Draw (version 2021) was used to prepare the figures.

References

1. Newbold, C., Craig, A., Kyes, S., Rowe, A., Fernandez-Reyes, D., and Fagan, T. (1999). Cytoadherence, pathogenesis and the infected red cell surface in Plasmodium falciparum. International Journal for Parasitology *29*, 927–937. https://doi.org/10.1016/S0020-7519(99)00049-1.

2. Borst, P., Bitter, W., McCulloch, R., Van Leeuwen, F., and Rudenko, G. (1995). Antigenic variation in malaria. Cell *82*, 1–4. https://doi.org/10.1016/0092-8674(95)90044-6.

3. Miller, L.H., Baruch, D.I., Marsh, K., and Doumbo, O.K. (2002). The pathogenic basis of malaria. Nature *415*, 673–679. https://doi.org/10.1038/415673a.

4. Baruch, D.I., Pasloske, B.L., Singh, H.B., Bi, X., Ma, X.C., Feldman, M., Taraschi, T.F., and Howard, R.J. (1995). Cloning the P. falciparum gene encoding PfEMP1, a malarial variant antigen and adherence receptor on the surface of parasitized human erythrocytes. Cell *82*, 77–87. https://doi.org/10.1016/0092-8674(95)90054-3.

5. Gardner, M.J., Hall, N., Fung, E., White, O., Berriman, M., Hyman, R.W., Carlton, J.M., Pain, A., Nelson, K.E., Bowman, S., et al. (2002). Genome sequence of the human malaria parasite Plasmodium falciparum. Nature *419*, 498–511. https://doi.org/10.1038/nature01097.

6. Leech, J.H., Barnwell, J.W., Miller, L.H., and Howard, R.J. (1984). Identification of a strain-specific malarial antigen exposed on the surface of Plasmodium falciparum-infected erythrocytes. J Exp Med *159*, 1567–1575. https://doi.org/10.1084/jem.159.6.1567.

7. Smith, J.D., Chitnis, C.E., Craig, A.G., Roberts, D.J., Hudson-Taylor, D.E., Peterson, D.S., Pinches, R., Newbold, C.I., and Miller, L.H. (1995). Switches in expression of Plasmodium falciparum var genes correlate with changes in antigenic and cytoadherent phenotypes of infected erythrocytes. Cell *82*, 101–110. https://doi.org/10.1016/0092-8674(95)90056-x.

8. Kyes, S.A., Kraemer, S.M., and Smith, J.D. (2007). Antigenic Variation in Plasmodium falciparum: Gene Organization and Regulation of the var Multigene Family. Eukaryot Cell *6*, 1511–1520. https://doi.org/10.1128/EC.00173-07.

9. Salanti, A., Dahlbäck, M., Turner, L., Nielsen, M.A., Barfod, L., Magistrado, P., Jensen, A.T.R., Lavstsen, T., Ofori, M.F., Marsh, K., et al. (2004). Evidence for the Involvement of VAR2CSA in Pregnancy-associated Malaria. J Exp Med *200*, 1197–1203. https://doi.org/10.1084/jem.20041579.

10. Salanti, A., Staalsoe, T., Lavstsen, T., Jensen, A.T.R., Sowa, M.P.K., Arnot, D.E., Hviid, L., and Theander, T.G. (2003). Selective upregulation of a single distinctly structured var gene in chondroitin sulphate A-adhering Plasmodium falciparum involved in pregnancy-associated malaria. Mol Microbiol *49*, 179–191. https://doi.org/10.1046/j.1365-2958.2003.03570.x.

11. Scherf, A., Hernandez-Rivas, R., Buffet, P., Bottius, E., Benatar, C., Pouvelle, B., Gysin, J., and Lanzer, M. (1998). Antigenic variation in malaria: in situ switching, relaxed and mutually exclusive transcription of var genes during intra-erythrocytic development in Plasmodium falciparum. EMBO J *17*, 5418–5426. https://doi.org/10.1093/emboj/17.18.5418.

12. Smith, J.D. (2014). The role of PfEMP1 adhesion domain classification in Plasmodium falciparum pathogenesis research. Mol Biochem Parasitol *195*, 82–87. https://doi.org/10.1016/j.molbiopara.2014.07.006.

13. Turner, L., Lavstsen, T., Berger, S.S., Wang, C.W., Petersen, J.E.V., Avril, M., Brazier, A.J., Freeth, J., Jespersen, J.S., Nielsen, M.A., et al. (2013). Severe malaria is associated with parasite binding to endothelial protein C receptor. Nature *498*, 502–505. https://doi.org/10.1038/nature12216.

14. Ruangjirachuporn, W., Afzelius, B.A., Helmby, H., Hill, A.V., Greenwood, B.M., Carlson, J., Berzins, K., Perlmann, P., and Wahlgren, M. (1992). Ultrastructural analysis of fresh Plasmodium falciparum-infected erythrocytes and their cytoadherence to human leukocytes. Am J Trop Med Hyg *46*, 511–519. https://doi.org/10.4269/ajtmh.1992.46.511.

15. Crabb, B.S., Cooke, B.M., Reeder, J.C., Waller, R.F., Caruana, S.R., Davern, K.M., Wickham, M.E., Brown, G.V., Coppel, R.L., and Cowman, A.F. (1997). Targeted gene disruption shows that knobs enable malaria-infected red cells to cytoadhere under physiological shear stress. Cell *89*, 287–296. https://doi.org/10.1016/s0092-8674(00)80207-x.

16. Sanchez, C.P., Karathanasis, C., Sanchez, R., Cyrklaff, M., Jäger, J., Buchholz, B., Schwarz, U.S., Heilemann, M., and Lanzer, M. (2019). Single-molecule imaging and quantification of the immune-variant adhesin VAR2CSA on knobs of Plasmodium falciparum-infected erythrocytes. Commun Biol *2*, 1–9. https://doi.org/10.1038/s42003-019-0429-z.

17. Otto, T.D., Assefa, S.A., Böhme, U., Sanders, M.J., Kwiatkowski, D., Berriman, M., and Newbold, C. (2019). Evolutionary analysis of the most polymorphic gene family in falciparum malaria. Wellcome Open Res *4*, 193. https://doi.org/10.12688/wellcomeopenres.15590.1.

18. Rask, T.S., Hansen, D.A., Theander, T.G., Gorm Pedersen, A., and Lavstsen, T. (2010). Plasmodium falciparum Erythrocyte Membrane Protein 1 Diversity in Seven Genomes – Divide and Conquer. PLoS Comput Biol *6*, e1000933. https://doi.org/10.1371/journal.pcbi.1000933.

19. Thompson, J.K., Rubio, J.P., Caruana, S., Brockman, A., Wickham, M.E., and Cowman, A.F. (1997). The chromosomal organization of the Plasmodium falciparum var gene family is conserved. Molecular and Biochemical Parasitology *87*, 49–60. https://doi.org/10.1016/S0166-6851(97)00041-8.

20. Chen, Q., Fernandez, V., Sundström, A., Schlichtherle, M., Datta, S., Hagblom, P., and Wahlgren, M. (1998). Developmental selection of var gene expression in Plasmodium falciparum. Nature *394*, 392–395. https://doi.org/10.1038/28660.

21. Voss, T.S., Bozdech, Z., and Bártfai, R. (2014). Epigenetic memory takes center stage in the survival strategy of malaria parasites. Current Opinion in Microbiology *20*, 88–95. https://doi.org/10.1016/j.mib.2014.05.007.

22. Chan, J.-A., Howell, K.B., Reiling, L., Ataide, R., Mackintosh, C.L., Fowkes, F.J.I., Petter, M., Chesson, J.M., Langer, C., Warimwe, G.M., et al. (2012). Targets of antibodies against Plasmodium falciparum-infected erythrocytes in malaria immunity. J Clin Invest *122*, 3227–3238. https://doi.org/10.1172/JCI62182.

23. Bull, P.C., Lowe, B.S., Kortok, M., Molyneux, C.S., Newbold, C.I., and Marsh, K. (1998). Parasite antigens on the infected red cell surface are targets for naturally acquired immunity to malaria. Nat Med *4*, 358–360. https://doi.org/10.1038/nm0398-358.

24. Bull, P.C., and Marsh, K. (2002). The role of antibodies to Plasmodium falciparum-infected-erythrocyte surface antigens in naturally acquired immunity to malaria. Trends Microbiol *10*, 55–58. https://doi.org/10.1016/s0966-842x(01)02278-8.

25. Guizetti, J., and Scherf, A. (2013). Silence, activate, poise and switch! Mechanisms of antigenic variation in Plasmodium falciparum. Cell Microbiol *15*, 718–726. https://doi.org/10.1111/cmi.12115.

26. Kyes, S., Horrocks, P., and Newbold, C. (2001). Antigenic variation at the infected red cell surface in malaria. Annu Rev Microbiol *55*, 673–707. https://doi.org/10.1146/annurev.micro.55.1.673.

27. Wichers-Misterek, J.S., Krumkamp, R., Held, J., von Thien, H., Wittmann, I., Höppner, Y.D., Ruge, J.M., Moser, K., Dara, A., Strauss, J., et al. (2023). The exception that proves the rule: Virulence gene expression at the onset of Plasmodium falciparum blood stage infections. PLoS Pathog *19*, e1011468. https://doi.org/10.1371/journal.ppat.1011468.

28. Smith, J.D., Rowe, J.A., Higgins, M.K., and Lavstsen, T. (2013). Malaria's Deadly Grip: Cytoadhesion of Plasmodium falciparum Infected Erythrocytes. Cell Microbiol *15*, 10.1111/cmi.12183. https://doi.org/10.1111/cmi.12183.

29. Wichers, J.S., Tonkin-Hill, G., Thye, T., Krumkamp, R., Kreuels, B., Strauss, J., von Thien, H., Scholz, J.A., Smedegaard Hansson, H., Weisel Jensen, R., et al. (2021). Common virulence gene expression in adult first-time infected malaria patients and severe cases. Elife *10*, e69040. https://doi.org/10.7554/eLife.69040.

30. Batinovic, S., McHugh, E., Chisholm, S.A., Matthews, K., Liu, B., Dumont, L., Charnaud, S.C., Schneider, M.P., Gilson, P.R., de Koning-Ward, T.F., et al. (2017). An exported protein-interacting complex involved in the trafficking of virulence determinants in Plasmodium-infected erythrocytes. Nat Commun *8*, 16044. https://doi.org/10.1038/ncomms16044.

31. Beck, J.R., Muralidharan, V., Oksman, A., and Goldberg, D.E. (2014). PTEX component HSP101 mediates export of diverse malaria effectors into host erythrocytes. Nature *511*, 592–595. https://doi.org/10.1038/nature13574.

32. de Koning-Ward, T.F., Gilson, P.R., Boddey, J.A., Rug, M., Smith, B.J., Papenfuss, A.T., Sanders, P.R., Lundie, R.J., Maier, A.G., Cowman, A.F., et al. (2009). A newly discovered protein export machine in malaria parasites. Nature *459*, 945–949. https://doi.org/10.1038/nature08104.

33. Elsworth, B., Matthews, K., Nie, C.Q., Kalanon, M., Charnaud, S.C., Sanders, P.R., Chisholm, S.A., Counihan, N.A., Shaw, P.J., Pino, P., et al. (2014). PTEX is an essential nexus for protein export in malaria parasites. Nature *511*, 587–591. https://doi.org/10.1038/nature13555.

34. McMillan, P.J., Millet, C., Batinovic, S., Maiorca, M., Hanssen, E., Kenny, S., Muhle, R.A., Melcher, M., Fidock, D.A., Smith, J.D., et al. (2013). Spatial and temporal mapping of the PfEMP1 export pathway in Plasmodium falciparum. Cell Microbiol *15*, 1401–1418. https://doi.org/10.1111/cmi.12125.

35. Riglar, D.T., Rogers, K.L., Hanssen, E., Turnbull, L., Bullen, H.E., Charnaud, S.C., Przyborski, J., Gilson, P.R., Whitchurch, C.B., Crabb, B.S., et al. (2013). Spatial association with PTEX complexes defines regions for effector export into Plasmodium falciparum-infected erythrocytes. Nat Commun *4*, 1415. https://doi.org/10.1038/ncomms2449.

36. Carmo, O.M.S., Shami, G.J., Cox, D., Liu, B., Blanch, A.J., Tiash, S., Tilley, L., and Dixon, M.W.A. (2022). Deletion of the Plasmodium falciparum exported protein PTP7 leads to Maurer's clefts vesiculation, host cell remodeling defects, and loss of surface presentation of EMP1. PLOS Pathogens *18*, e1009882. https://doi.org/10.1371/journal.ppat.1009882.

37. Cooke, B.M., Buckingham, D.W., Glenister, F.K., Fernandez, K.M., Bannister, L.H., Marti, M., Mohandas, N., and Coppel, R.L. (2006). A Maurer's cleft–associated protein is essential for expression of the major malaria virulence antigen on the surface of infected red blood cells. J Cell Biol *172*, 899–908. https://doi.org/10.1083/jcb.200509122.

38. Maier, A.G., Rug, M., O'Neill, M.T., Beeson, J.G., Marti, M., Reeder, J., and Cowman, A.F. (2007). Skeleton-binding protein 1 functions at the parasitophorous vacuole membrane to traffic PfEMP1 to the Plasmodium falciparum–infected erythrocyte surface. Blood *109*, 1289–1297. https://doi.org/10.1182/blood-2006-08-043364.

39. Rug, M., Cyrklaff, M., Mikkonen, A., Lemgruber, L., Kuelzer, S., Sanchez, C.P., Thompson, J., Hanssen, E., O'Neill, M., Langer, C., et al. (2014). Export of virulence proteins by malaria-infected erythrocytes involves remodeling of host actin cytoskeleton. Blood *124*, 3459–3468. https://doi.org/10.1182/blood-2014-06-583054.

40. Avril, M., Tripathi, A.K., Brazier, A.J., Andisi, C., Janes, J.H., Soma, V.L., Sullivan, D.J., Bull, P.C., Stins, M.F., and Smith, J.D. (2012). A restricted subset of var genes mediates adherence of Plasmodium falciparum-infected erythrocytes to brain endothelial cells. Proc Natl Acad Sci U S A *109*, E1782-1790. https://doi.org/10.1073/pnas.1120534109.

41. Claessens, A., Adams, Y., Ghumra, A., Lindergard, G., Buchan, C.C., Andisi, C., Bull, P.C., Mok, S., Gupta, A.P., Wang, C.W., et al. (2012). A subset of group A-like var genes encodes the malaria parasite ligands for binding to human brain endothelial cells. Proc Natl Acad Sci U S A *109*, E1772–E1781. https://doi.org/10.1073/pnas.1120461109.

42. Cooke, B.M., Rogerson, S.J., Brown, G.V., and Coppel, R.L. (1996). Adhesion of Malaria-Infected Red Blood Cells to Chondroitin Sulfate A Under Flow Conditions. Blood *88*, 4040–4044. https://doi.org/10.1182/blood.V88.10.4040.bloodjournal88104040.

43. Nunes-Silva, S., Dechavanne, S., Moussiliou, A., Pstrąg, N., Semblat, J.-P., Gangnard, S., Tuikue-Ndam, N., Deloron, P., Chêne, A., and Gamain, B. (2015). Beninese children with cerebral malaria do not develop humoral immunity against the IT4-VAR19-DC8 PfEMP1 variant linked to EPCR and brain endothelial binding. Malar J *14*, 493. https://doi.org/10.1186/s12936-015-1008-5.

44. Maier, A.G., Rug, M., O'Neill, M.T., Brown, M., Chakravorty, S., Szestak, T., Chesson, J., Wu, Y., Hughes, K., Coppel, R.L., et al. (2008). Exported proteins required for virulence and rigidity of Plasmodium falciparum-infected human erythrocytes. Cell *134*, 48–61. https://doi.org/10.1016/j.cell.2008.04.051.

45. Nilsson, S., Angeletti, D., Wahlgren, M., Chen, Q., and Moll, K. (2012). Plasmodium falciparum Antigen 332 Is a Resident Peripheral Membrane Protein of Maurer's Clefts. PLoS One *7*, e46980. https://doi.org/10.1371/journal.pone.0046980.

46. Looker, O., Blanch, A.J., Liu, B., Nunez-Iglesias, J., McMillan, P.J., Tilley, L., and Dixon, M.W.A. (2019). The knob protein KAHRP assembles into a ring-shaped structure that underpins virulence complex assembly. PLoS Pathog *15*, e1007761. https://doi.org/10.1371/journal.ppat.1007761.

47. Melcher, M., Muhle, R.A., Henrich, P.P., Kraemer, S.M., Avril, M., Vigan-Womas, I., Mercereau-Puijalon, O., Smith, J.D., and Fidock, D.A. (2010). Identification of a Role for the PfEMP1 Semi-Conserved Head Structure in Protein Trafficking to the Surface of Plasmodium falciparum Infected Red Blood Cells. Cell Microbiol *12*, 1446–1462. https://doi.org/10.1111/j.1462-5822.2010.01481.x.

48. Birnbaum, J., Flemming, S., Reichard, N., Soares, A.B., Mesén-Ramírez, P., Jonscher, E., Bergmann, B., and Spielmann, T. (2017). A genetic system to study Plasmodium falciparum protein function. Nat Methods *14*, 450–456. https://doi.org/10.1038/nmeth.4223.

49. Omelianczyk, R.I., Loh, H.P., Chew, M., Hoo, R., Baumgarten, S., Renia, L., Chen, J., and Preiser, P.R. (2020). Rapid activation of distinct members of multigene families in Plasmodium spp. Commun Biol *3*, 1–11. https://doi.org/10.1038/s42003-020-1081-3.

50. Waterkeyn, J.G., Wickham, M.E., Davern, K.M., Cooke, B.M., Coppel, R.L., Reeder, J.C., Culvenor, J.G., Waller, R.F., and Cowman, A.F. (2000). Targeted mutagenesis of Plasmodium falciparum erythrocyte membrane protein 3 (PfEMP3) disrupts cytoadherence of malaria-infected red blood cells. EMBO J *19*, 2813–2823. https://doi.org/10.1093/emboj/19.12.2813.

51. Joergensen, L., Bengtsson, D.C., Bengtsson, A., Ronander, E., Berger, S.S., Turner, L., Dalgaard, M.B., Cham, G.K.K., Victor, M.E., Lavstsen, T., et al. (2010). Surface Co-Expression of Two Different PfEMP1 Antigens on Single Plasmodium falciparum-Infected Erythrocytes Facilitates Binding to ICAM1 and PECAM1. PLoS Pathog *6*, e1001083. https://doi.org/10.1371/journal.ppat.1001083.

52. Flueck, C., Bartfai, R., Niederwieser, I., Witmer, K., Alako, B.T.F., Moes, S., Bozdech, Z., Jenoe, P., Stunnenberg, H.G., and Voss, T.S. (2010). A major role for the Plasmodium falciparum ApiAP2 protein PfSIP2 in chromosome end biology. PLoS Pathog *6*, e1000784. https://doi.org/10.1371/journal.ppat.1000784.

53. Guizetti, J., Barcons-Simon, A., and Scherf, A. (2016). Trans-acting GC-rich non-coding RNA at var expression site modulates gene counting in malaria parasite. Nucleic Acids Res *44*, 9710–9718. https://doi.org/10.1093/nar/gkw664.

54. Eilers, M., and Schatz, G. (1986). Binding of a specific ligand inhibits import of a purified precursor protein into mitochondria. Nature *322*, 228–232. https://doi.org/10.1038/322228a0.

55. Gehde, N., Hinrichs, C., Montilla, I., Charpian, S., Lingelbach, K., and Przyborski, J.M. (2009). Protein unfolding is an essential requirement for transport across the parasitophorous vacuolar membrane of Plasmodium falciparum. Mol Microbiol *71*, 613–628. https://doi.org/10.1111/j.1365-2958.2008.06552.x.

56. Grüring, C., Heiber, A., Kruse, F., Flemming, S., Franci, G., Colombo, S.F., Fasana, E., Schoeler, H., Borgese, N., Stunnenberg, H.G., et al. (2012). Uncovering Common Principles in Protein Export of Malaria Parasites. Cell Host & Microbe *12*, 717–729. https://doi.org/10.1016/j.chom.2012.09.010.

57. Mesén-Ramírez, P., Reinsch, F., Soares, A.B., Bergmann, B., Ullrich, A.-K., Tenzer, S., and Spielmann, T. (2016). Stable Translocation Intermediates Jam Global Protein Export in Plasmodium falciparum Parasites and Link the PTEX Component EXP2 with Translocation Activity. PLOS Pathogens *12*, e1005618. https://doi.org/10.1371/journal.ppat.1005618.

58. Grüring, C., Heiber, A., Kruse, F., Ungefehr, J., Gilberger, T.-W., and Spielmann, T. (2011). Development and host cell modifications of Plasmodium falciparum blood stages in four dimensions. Nat Commun *2*, 165. https://doi.org/10.1038/ncomms1169.

59. Marti, M., Good, R.T., Rug, M., Knuepfer, E., and Cowman, A.F. (2004). Targeting malaria virulence and remodeling proteins to the host erythrocyte. Science *306*, 1930–1933. https://doi.org/10.1126/science.1102452.

60. Bourke, P.F., Holt, D.C., Sutherland, C.J., and Kemp, D.J. (1996). Disruption of a novel open reading frame of Plasmodium falciparum chromosome 9 by subtelomeric and internal deletions can lead to loss or maintenance of cytoadherence. Mol Biochem Parasitol *82*, 25–36. https://doi.org/10.1016/0166-6851(96)02715-6.

61. Udeinya, I.J., Graves, P.M., Carter, R., Aikawa, M., and Miller, L.H. (1983). Plasmodium falciparum: effect of time in continuous culture on binding to human endothelial cells and amelanotic melanoma cells. Exp Parasitol *56*, 207–214. https://doi.org/10.1016/0014-4894(83)90064-4.

62. Hsieh, F.-L., Turner, L., Bolla, J.R., Robinson, C.V., Lavstsen, T., and Higgins, M.K. (2016). The structural basis for CD36 binding by the malaria parasite. Nat Commun *7*, 12837. https://doi.org/10.1038/ncomms12837.

63. Howell, D.P.-G., Levin, E.A., Springer, A.L., Kraemer, S.M., Phippard, D.J., Schief, W.R., and Smith, J.D. (2008). Mapping a common interaction site used by Plasmodium falciparum Duffy binding-like domains to bind diverse host receptors. Molecular Microbiology *67*, 78–87. https://doi.org/10.1111/j.1365-2958.2007.06019.x.

64. Janes, J.H., Wang, C.P., Levin-Edens, E., Vigan-Womas, I., Guillotte, M., Melcher, M., Mercereau-Puijalon, O., and Smith, J.D. (2011). Investigating the Host Binding Signature on the Plasmodium falciparum PfEMP1 Protein Family. PLoS Pathog *7*, e1002032. https://doi.org/10.1371/journal.ppat.1002032.

65. Metwally, N.G., Tilly, A.-K., Lubiana, P., Roth, L.K., Dörpinghaus, M., Lorenzen, S., Schuldt, K., Witt, S., Bachmann, A., Tidow, H., et al. (2017). Characterisation of Plasmodium falciparum populations selected on the human endothelial receptors P-selectin, E-selectin, CD9 and CD151. Sci Rep *7*, 4069. https://doi.org/10.1038/s41598-017-04241-3.

66. Adams, Y., Olsen, R.W., Bengtsson, A., Dalgaard, N., Zdioruk, M., Satpathi, S., Behera, P.K., Sahu, P.K., Lawler, S.E., Qvortrup, K., et al. (2021). Plasmodium falciparum erythrocyte membrane protein 1 variants induce cell swelling and disrupt the blood-brain barrier in cerebral malaria. J Exp Med *218*, e20201266. https://doi.org/10.1084/jem.20201266.

67. Blancke Soares, A., Stäcker, J., Schwald, S., Hoijmakers, W., Metwally, N.G., Cronshagen, J., Schoeler, H., Flemming, S., Höhn, K., Fröhlke, U., et al. (2025). An unusual trafficking domain in MSRP6 defines a complex needed for Maurer's clefts anchoring and maintenance in P. falciparum infected red blood cells. Preprint, https://doi.org/10.7554/eLife.103633.1 https://doi.org/10.7554/eLife.103633.1.

68. Roux, K.J., Kim, D.I., Raida, M., and Burke, B. (2012). A promiscuous biotin ligase fusion protein identifies proximal and interacting proteins in mammalian cells. J Cell Biol *196*, 801–810. https://doi.org/10.1083/jcb.201112098.

69. Sargeant, T.J., Marti, M., Caler, E., Carlton, J.M., Simpson, K., Speed, T.P., and Cowman, A.F. (2006). Lineage-specific expansion of proteins exported to erythrocytes in malaria parasites. Genome Biology *7*, R12. https://doi.org/10.1186/gb-2006-7-2-r12.

70. Marti, M., and Spielmann, T. (2013). Protein export in malaria parasites: many membranes to cross. Curr Opin Microbiol *16*, 445–451. https://doi.org/10.1016/j.mib.2013.04.010.

71. Papakrivos, J., Newbold, C.I., and Lingelbach, K. (2005). A potential novel mechanism for the insertion of a membrane protein revealed by a biochemical analysis of the Plasmodium falciparum cytoadherence molecule PfEMP-1. Mol Microbiol *55*, 1272–1284. https://doi.org/10.1111/j.1365-2958.2004.04468.x.

72. Petersen, W., Külzer, S., Engels, S., Zhang, Q., Ingmundson, A., Rug, M., Maier, A.G., and Przyborski, J.M. (2016). J-dot targeting of an exported HSP40 in *Plasmodium falciparum*-infected erythrocytes. International Journal for Parasitology *46*, 519–525. https://doi.org/10.1016/j.ijpara.2016.03.005.

73. Chan, S., Frasch, A., Mandava, C.S., Ch'ng, J.-H., Quintana, M.D.P., Vesterlund, M., Ghorbal, M., Joannin, N., Franzén, O., Lopez-Rubio, J.-J., et al. (2017). Regulation of PfEMP1-VAR2CSA translation by a Plasmodium translation-enhancing factor. Nat Microbiol *2*, 17068. https://doi.org/10.1038/nmicrobiol.2017.68.

74. Dantzler, K.W., Ma, S., Ngotho, P., Stone, W.J.R., Tao, D., Rijpma, S., De Niz, M., Nilsson Bark, S.K., Jore, M.M., Raaijmakers, T.K., et al. (2019). Naturally acquired immunity against immature Plasmodium falciparum gametocytes. Science Translational Medicine *11*, eaav3963. https://doi.org/10.1126/scitranslmed.aav3963.

75. Davies, H., Belda, H., Broncel, M., Dalimot, J., and Treeck, M. (2023). PerTurboID, a targeted in situ method reveals the impact of kinase deletion on its local protein environment in the cytoadhesion complex of malaria-causing parasites. eLife *12*, e86367. https://doi.org/10.7554/eLife.86367.

76. Hermand, P., Cicéron, L., Pionneau, C., Vaquero, C., Combadière, C., and Deterre, P. (2016). Plasmodium falciparum proteins involved in cytoadherence of infected erythrocytes to chemokine CX3CL1. Sci Rep *6*, 33786. https://doi.org/10.1038/srep33786.

77. Tarr, S.J., Moon, R.W., Hardege, I., and Osborne, A.R. (2014). A conserved domain targets exported PHISTb family proteins to the periphery of Plasmodium infected erythrocytes. Mol Biochem Parasitol *196*, 29–40. https://doi.org/10.1016/j.molbiopara.2014.07.011.

78. Pachlatko, E., Rusch, S., Müller, A., Hemphill, A., Tilley, L., Hanssen, E., and Beck, H.-P. (2010). MAHRP2, an exported protein of Plasmodium falciparum, is an essential component of Maurer's cleft tethers. Molecular Microbiology *77*, 1136–1152. https://doi.org/10.1111/j.1365-2958.2010.07278.x.

79. Külzer, S., Charnaud, S., Dagan, T., Riedel, J., Mandal, P., Pesce, E.R., Blatch, G.L., Crabb, B.S., Gilson, P.R., and Przyborski, J.M. (2012). Plasmodium falciparum-encoded exported hsp70/hsp40 chaperone/co-chaperone complexes within the host erythrocyte. Cell Microbiol *14*, 1784–1795. https://doi.org/10.1111/j.1462-5822.2012.01840.x.

80. Zhang, Q., Ma, C., Oberli, A., Zinz, A., Engels, S., and Przyborski, J.M. (2017). Proteomic analysis of exported chaperone/co-chaperone complexes of P. falciparum reveals an array of complex protein-protein interactions. Sci Rep *7*, 42188. https://doi.org/10.1038/srep42188.

81. Schulze, J., Kwiatkowski, M., Borner, J., Schlüter, H., Bruchhaus, I., Burmester, T., Spielmann, T., and Pick, C. (2015). The Plasmodium falciparum exportome contains non-canonical PEXEL/HT proteins. Mol Microbiol *97*, 301–314. https://doi.org/10.1111/mmi.13024.

82. Heiber, A., Kruse, F., Pick, C., Grüring, C., Flemming, S., Oberli, A., Schoeler, H., Retzlaff, S., Mesén-Ramírez, P., Hiss, J.A., et al. (2013). Identification of New PNEPs Indicates a Substantial Non-PEXEL Exportome and Underpins Common Features in Plasmodium falciparum Protein Export. PLOS Pathogens *9*, e1003546. https://doi.org/10.1371/journal.ppat.1003546.

83. McMillan, P.J., Millet, C., Batinovic, S., Maiorca, M., Hanssen, E., Kenny, S., Muhle, R.A., Melcher, M., Fidock, D.A., Smith, J.D., et al. (2013). Spatial and temporal mapping of the PfEMP1 export pathway in Plasmodium falciparum. Cellular Microbiology *15*, 1401–1418. https://doi.org/10.1111/cmi.12125.

84. Wu, B., Rambow, J., Bock, S., Holm-Bertelsen, J., Wiechert, M., Soares, A.B., Spielmann, T., and Beitz, E. (2015). Identity of a Plasmodium lactate/H+ symporter structurally unrelated to human transporters. Nat Commun *6*, 6284. https://doi.org/10.1038/ncomms7284.

85. Marchetti, R.V., Lehane, A.M., Shafik, S.H., Winterberg, M., Martin, R.E., and Kirk, K. (2015). A lactate and formate transporter in the intraerythrocytic malaria parasite, Plasmodium falciparum. Nat Commun *6*, 6721. https://doi.org/10.1038/ncomms7721.

86. Golldack, A., Henke, B., Bergmann, B., Wiechert, M., Erler, H., Blancke Soares, A., Spielmann, T., and Beitz, E. (2017). Substrate-analogous inhibitors exert antimalarial action by targeting the Plasmodium lactate transporter PfFNT at nanomolar scale. PLoS Pathog *13*, e1006172. https://doi.org/10.1371/journal.ppat.1006172.

87. Walloch, P., Henke, B., Häuer, S., Bergmann, B., Spielmann, T., and Beitz, E. (2020). Introduction of Scaffold Nitrogen Atoms Renders Inhibitors of the Malarial l-Lactate Transporter, PfFNT, Effective against the Gly107Ser Resistance Mutation. J Med Chem *63*, 9731–9741. https://doi.org/10.1021/acs.jmedchem.0c00852.

88. Rajan Raghavan, S.S., Turner, L., Jensen, R.W., Johansen, N.T., Jensen, D.S., Gourdon, P., Zhang, J., Wang, Y., Theander, T.G., Wang, K., et al. (2023). Endothelial protein C receptor binding induces conformational changes to severe malaria-associated group A PfEMP1. Structure *31*, 1174-1183.e4. https://doi.org/10.1016/j.str.2023.07.011.

89. Reyes, R.A., Raghavan, S.S.R., Hurlburt, N.K., Introini, V., Kana, I.H., Jensen, R.W., Martinez-Scholze, E., Gestal-Mato, M., Bau, C.B., Fernández-Quintero, M.L., et al. (2024). Broadly inhibitory antibodies against severe malaria virulence proteins. Preprint at bioRxiv, https://doi.org/10.1101/2024.01.25.577124 https://doi.org/10.1101/2024.01.25.577124.

90. Gillrie, M.R., Avril, M., Brazier, A.J., Davis, S.P., Stins, M.F., Smith, J.D., and Ho, M. (2015). Diverse functional outcomes of Plasmodium falciparum ligation of EPCR: potential implications for malarial pathogenesis. Cellular Microbiology *17*, 1883–1899. https://doi.org/10.1111/cmi.12479.

91. Ortolan, L.S., Avril, M., Xue, J., Seydel, K.B., Zheng, Y., and Smith, J.D. (2022). Plasmodium falciparum Parasite Lines Expressing DC8 and Group A PfEMP1 Bind to Brain, Intestinal, and Kidney Endothelial Cells. Front Cell Infect Microbiol *12*, 813011. https://doi.org/10.3389/fcimb.2022.813011.

92. Culvenor, J.G., Langford, C.J., Crewther, P.E., Saint, R.B., Coppel, R.L., Kemp, D.J., Anders, R.F., and Brown, G.V. (1987). Plasmodium falciparum: identification and localization of a knob protein antigen expressed by a cDNA clone. Exp Parasitol *63*, 58–67. https://doi.org/10.1016/0014-4894(87)90078-6.

93. Pologe, L.G., Pavlovec, A., Shio, H., and Ravetch, J.V. (1987). Primary structure and subcellular localization of the knob-associated histidine-rich protein of Plasmodium falciparum. Proc Natl Acad Sci U S A *84*, 7139–7143.

94. Rug, M., Prescott, S.W., Fernandez, K.M., Cooke, B.M., and Cowman, A.F. (2006). The role of KAHRP domains in knob formation and cytoadherence of P falciparum-infected human erythrocytes. Blood *108*, 370–378. https://doi.org/10.1182/blood-2005-11-4624.

95. Oh, S.S., Voigt, S., Fisher, D., Yi, S.J., LeRoy, P.J., Derick, L.H., Liu, S., and Chishti, A.H. (2000). Plasmodium falciparum erythrocyte membrane protein 1 is anchored to the actin-spectrin junction and knob-associated histidine-rich protein in the erythrocyte skeleton. Mol Biochem Parasitol *108*, 237–247. https://doi.org/10.1016/s0166-6851(00)00227-9.

96. Waller, K.L., Cooke, B.M., Nunomura, W., Mohandas, N., and Coppel, R.L. (1999). Mapping the binding domains involved in the interaction between the Plasmodium falciparum knob-associated histidine-rich protein (KAHRP) and the cytoadherence ligand P. falciparum erythrocyte membrane protein 1 (PfEMP1). J Biol Chem *274*, 23808–23813. https://doi.org/10.1074/jbc.274.34.23808.

97. Waller, R.F., Reed, M.B., Cowman, A.F., and McFadden, G.I. (2000). Protein trafficking to the plastid of Plasmodium falciparum is via the secretory pathway. EMBO J *19*, 1794–1802. https://doi.org/10.1093/emboj/19.8.1794.

98. Mayer, C., Slater, L., Erat, M.C., Konrat, R., and Vakonakis, I. (2012). Structural Analysis of the Plasmodium falciparum Erythrocyte Membrane Protein 1 (PfEMP1) Intracellular Domain Reveals a Conserved Interaction Epitope. J Biol Chem *287*, 7182–7189. https://doi.org/10.1074/jbc.M111.330779.

99. Takano, R., Kozuka-Hata, H., Kondoh, D., Bochimoto, H., Oyama, M., and Kato, K. (2019). A High-Resolution Map of SBP1 Interactomes in Plasmodium falciparum-infected Erythrocytes. iScience *19*, 703–714. https://doi.org/10.1016/j.isci.2019.07.035.

100. Gabelich, J.-A., Grützke, J., Kirscht, F., Popp, O., Matz, J.M., Dittmar, G., Rug, M., and Ingmundson, A. (2022). A member of the tryptophan-rich protein family is required for efficient sequestration of Plasmodium berghei schizonts. PLoS Pathog *18*, e1010846. https://doi.org/10.1371/journal.ppat.1010846.

101. De Niz, M., Ullrich, A.-K., Heiber, A., Blancke Soares, A., Pick, C., Lyck, R., Keller, D., Kaiser, G., Prado, M., Flemming, S., et al. (2016). The machinery underlying malaria parasite virulence is conserved between rodent and human malaria parasites. Nat Commun *7*, 11659. https://doi.org/10.1038/ncomms11659.

102. Edgar, R., Domrachev, M., and Lash, A.E. (2002). Gene Expression Omnibus: NCBI gene expression and hybridization array data repository. Nucleic Acids Res *30*, 207–210. https://doi.org/10.1093/nar/30.1.207.

103. Perez-Riverol, Y., Bai, J., Bandla, C., García-Seisdedos, D., Hewapathirana, S., Kamatchinathan, S., Kundu, D.J., Prakash, A., Frericks-Zipper, A., Eisenacher, M., et al. (2022). The PRIDE database resources in 2022: a hub for mass spectrometry-based proteomics evidences. Nucleic Acids Res *50*, D543–D552. https://doi.org/10.1093/nar/gkab1038.

104. Gibson, D.G., Young, L., Chuang, R.-Y., Venter, J.C., Hutchison, C.A., and Smith, H.O. (2009). Enzymatic assembly of DNA molecules up to several hundred kilobases. Nat Methods *6*, 343–345. https://doi.org/10.1038/nmeth.1318.

105. Birnbaum, J., Scharf, S., Schmidt, S., Jonscher, E., Hoeijmakers, W.A.M., Flemming, S., Toenhake, C.G., Schmitt, M., Sabitzki, R., Bergmann, B., et al. (2020). A Kelch13-defined endocytosis pathway mediates artemisinin resistance in malaria parasites. Science *367*, 51–59. https://doi.org/10.1126/science.aax4735.

106. Walliker, D., Quakyi, I.A., Wellems, T.E., McCutchan, T.F., Szarfman, A., London, W.T., Corcoran, L.M., Burkot, T.R., and Carter, R. (1987). Genetic analysis of the human malaria parasite Plasmodium falciparum. Science *236*, 1661–1666. https://doi.org/10.1126/science.3299700.

107. Jensen, J.B., and Trager, W. (1978). Plasmodium falciparum in culture: establishment of additional strains. Am J Trop Med Hyg *27*, 743–746. https://doi.org/10.4269/ajtmh.1978.27.743.

108. Trager, W., and Jensen, J.B. (1976). Human malaria parasites in continuous culture. Science *193*, 673–675. https://doi.org/10.1126/science.781840.

109. Rivadeneira, E.M., Wasserman, M., and Espinal, C.T. (1983). Separation and concentration of schizonts of Plasmodium falciparum by Percoll gradients. J Protozool *30*, 367–370. https://doi.org/10.1111/j.1550-7408.1983.tb02932.x.

110. Moon, R.W., Hall, J., Rangkuti, F., Ho, Y.S., Almond, N., Mitchell, G.H., Pain, A., Holder, A.A., and Blackman, M.J. (2013). Adaptation of the genetically tractable malaria pathogen Plasmodium knowlesi to continuous culture in human erythrocytes. Proceedings of the National Academy of Sciences *110*, 531–536. https://doi.org/10.1073/pnas.1216457110.

111. Spielmann, T., Fergusen, D.J.P., and Beck, H.-P. (2003). etramps, a new Plasmodium falciparum gene family coding for developmentally regulated and highly charged membrane proteins located at the parasite-host cell interface. Mol Biol Cell *14*, 1529–1544. https://doi.org/10.1091/mbc.e02-04-0240.

112. Grüring, C., and Spielmann, T. (2012). Imaging of live malaria blood stage parasites. Methods Enzymol *506*, 81–92. https://doi.org/10.1016/B978-0-12-391856-7.00029-9.

113. Lambros, C., and Vanderberg, J.P. (1979). Synchronization of Plasmodium falciparum erythrocytic stages in culture. J Parasitol *65*, 418–420.

114. Heiber, A., and Spielmann, T. (2014). Preparation of Parasite Protein Extracts and Western Blot Analysis. BIO-PROTOCOL *4*. https://doi.org/10.21769/BioProtoc.1136.

115. Avril, M., Bernabeu, M., Benjamin, M., Brazier, A.J., and Smith, J.D. (2016). Interaction between Endothelial Protein C Receptor and Intercellular Adhesion Molecule 1 to Mediate Binding of Plasmodium falciparum-Infected Erythrocytes to Endothelial Cells. mBio *7*, e00615-16. https://doi.org/10.1128/mBio.00615-16.

116. Dahlbäck, M., Jørgensen, L.M., Nielsen, M.A., Clausen, T.M., Ditlev, S.B., Resende, M., Pinto, V.V., Arnot, D.E., Theander, T.G., and Salanti, A. (2011). The Chondroitin Sulfate A-binding Site of the VAR2CSA Protein Involves Multiple N-terminal Domains. J Biol Chem *286*, 15908–15917. https://doi.org/10.1074/jbc.M110.191510.

117. Renn, J.P., Doritchamou, J.Y.A., Tentokam, B.C.N., Morrison, R.D., Cowles, M.V., Burkhardt, M., Ma, R., Mahamar, A., Attaher, O., Diarra, B.S., et al. (2021). Allelic variants of full-length VAR2CSA, the placental malaria vaccine candidate, differ in antigenicity and receptor binding affinity. Commun Biol *4*, 1–12. https://doi.org/10.1038/s42003-021-02787-7.

118. Goodyer, I.D., Johnson, J., Eisenthal, R., and Hayes, D.J. (1994). Purification of mature-stage Plasmodium falciparum by gelatine flotation. Ann Trop Med Parasitol *88*, 209–211. https://doi.org/10.1080/00034983.1994.11812859.

119. Berg, S., Kutra, D., Kroeger, T., Straehle, C.N., Kausler, B.X., Haubold, C., Schiegg, M., Ales, J., Beier, T., Rudy, M., et al. (2019). ilastik: interactive machine learning for (bio)image analysis. Nat Methods *16*, 1226–1232. https://doi.org/10.1038/s41592-019-0582-9.

120. Stirling, D.R., Swain-Bowden, M.J., Lucas, A.M., Carpenter, A.E., Cimini, B.A., and Goodman, A. (2021). CellProfiler 4: improvements in speed, utility and usability. BMC Bioinformatics *22*, 433. https://doi.org/10.1186/s12859-021-04344-9.

121. Amos, B., Aurrecoechea, C., Barba, M., Barreto, A., Basenko, E.Y., Bażant, W., Belnap, R., Blevins, A.S., Böhme, U., Brestelli, J., et al. (2022). VEuPathDB: the eukaryotic pathogen, vector and host bioinformatics resource center. Nucleic Acids Research *50*, D898–D911. https://doi.org/10.1093/nar/gkab929.

122. Wang, C.W., Magistrado, P.A., Nielsen, M.A., Theander, T.G., and Lavstsen, T. (2009). Preferential transcription of conserved rif genes in two phenotypically distinct Plasmodium falciparum parasite lines. Int J Parasitol *39*, 655–664. https://doi.org/10.1016/j.ijpara.2008.11.014.

123. Hubner, N.C., Nguyen, L.N., Hornig, N.C., and Stunnenberg, H.G. (2015). A quantitative proteomics tool to identify DNA-protein interactions in primary cells or blood. J Proteome Res *14*, 1315–1329. https://doi.org/10.1021/pr5009515.

124. Rappsilber, J., Mann, M., and Ishihama, Y. (2007). Protocol for micro-purification, enrichment, pre-fractionation and storage of peptides for proteomics using StageTips. Nat Protoc *2*, 1896–1906. https://doi.org/10.1038/nprot.2007.261.

125. Cox, J., and Mann, M. (2008). MaxQuant enables high peptide identification rates, individualized p.p.b.-range mass accuracies and proteome-wide protein quantification. Nat Biotechnol *26*, 1367–1372. https://doi.org/10.1038/nbt.1511.

126. Tyanova, S., Temu, T., Sinitcyn, P., Carlson, A., Hein, M.Y., Geiger, T., Mann, M., and Cox, J. (2016). The Perseus computational platform for comprehensive analysis of (prote)omics data. Nat Methods *13*, 731–740. https://doi.org/10.1038/nmeth.3901.

127. Cui, Y., and Ma, L. (2018). Sequential use of milk and bovine serum albumin for streptavidin-probed western blot. BioTechniques *65*, 125–126. https://doi.org/10.2144/btn-2018-0006.

128. Behrens, H.M., Schmidt, S., Henshall, I.G., López-Barona, P., Peigney, D., Sabitzki, R., May, J., Maïga-Ascofaré, O., and Spielmann, T. (2024). Impact of different mutations on Kelch13 protein levels, ART resistance, and fitness cost in *Plasmodium falciparum* parasites. mBio *15*, e01981-23. https://doi.org/10.1128/mbio.01981-23.

129. Lord, S.J., Velle, K.B., Mullins, R.D., and Fritz-Laylin, L.K. (2020). SuperPlots: Communicating reproducibility and variability in cell biology. Journal of Cell Biology *219*, e202001064. https://doi.org/10.1083/jcb.202001064.

Figures

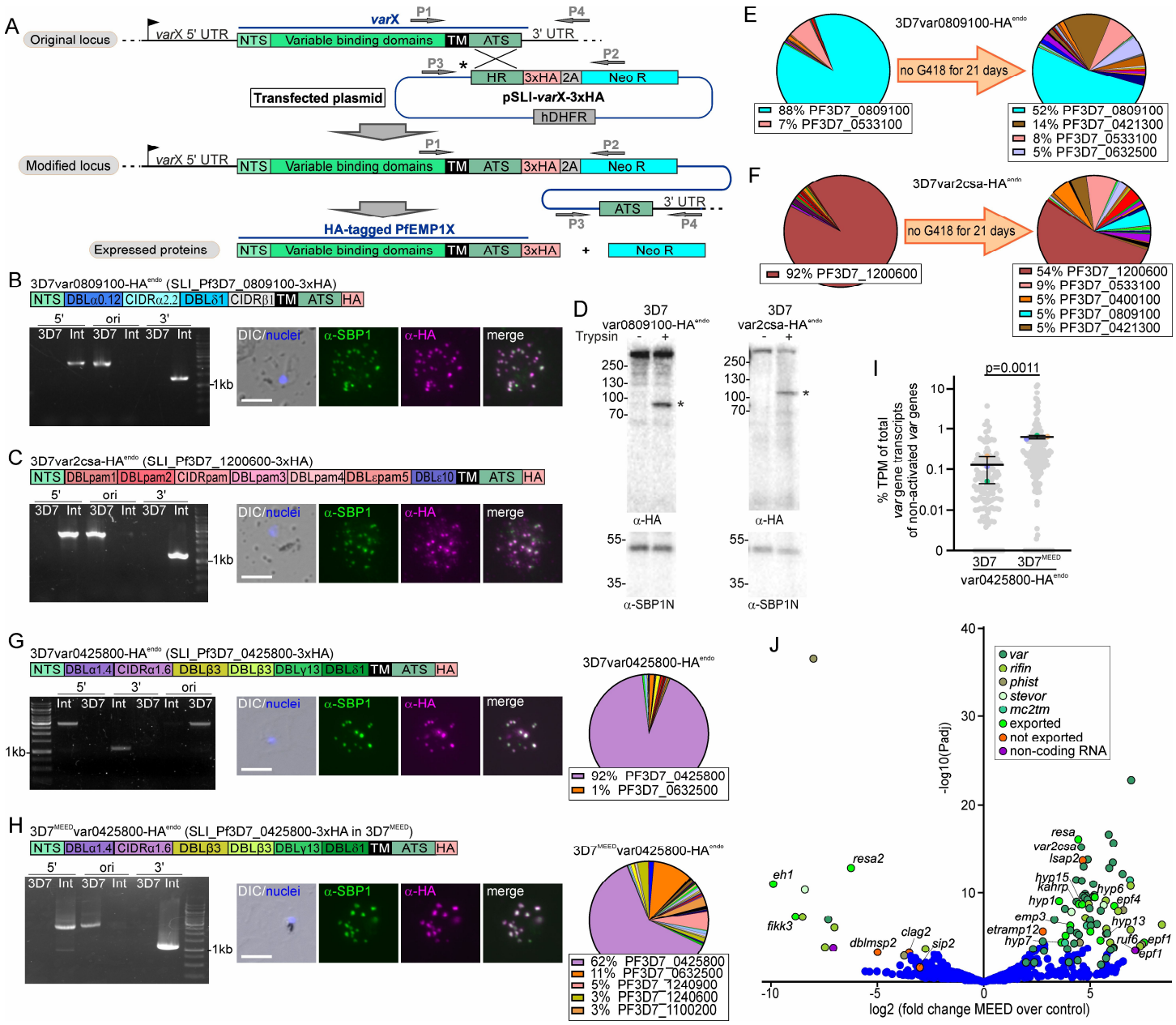

Figure 1. SLI-activation of *var* genes in 3D7. (A) Schematic for SLI strategy. HR: homology region; ATS: acidic terminal segment; NTS: N-terminal segment; 2A: T2A skip peptide; NEO-R: G418-resistance; hDHFR: human dihydrofolate reductase; arrows P1-4: primers for diagnostic PCR; X: desired *var* gene. (**B, C**) Activation of indicated PfEMP1. Scheme shows domain organisation. Agarose gels show PCR products confirming correct integration of the SLI plasmid. Product over 5´ integration junction (5'): P1+P2; 3' integration junction (3'): P3+P4; original locus (ori): P1+P4; see (A) for primer positions, see Table S6 for sequence of primers used; 3D7: parent; Int: integrant cell line. Fluorescence microscopy images show IFAs with indicated antibodies. Nuclei: Hoechst 33342; DIC: differential interference contrast; size bars 5 µm. (**D**) Western blot of trypsin cleavage assays with indicated parasites. Asterisks show protected PfEMP1 fragment. α-SBP1-N: control for integrity of host cell (breach of RBC membrane would result in a smaller SBP1 fragment). Marker in kDa. Replicates and full blots in Figure S4. (**E, F**) Pie charts with proportions of total *var* gene transcripts determined by qPCR of the indicated cell lines on G418 and after lifting G418. (**G, H**) Activation of PF3D7_0425800 in 3D7 or 3D7^{MEED}. Scheme shows domain organisation. Agarose gels show PCR products confirming

correct integration of the SLI plasmid as described in (A). Fluorescence microscopy images show IFAs as described in (B, C). Pie charts show proportions of total *var* gene transcripts of the indicated cell lines determined by RNAseq (normalized to TPM). (**I**) SuperPlot [129] showing percentage (log scale) of total *var* gene transcripts for non-activated *var* genes of the indicated cell line determined by RNAseq (normalized to TPM; small grey dots: individual *var* genes; large coloured dots: average of each replicate; bars: mean of averages of replicates with SD; n = 3 biological replicates; unpaired t-test; p-values indicated). See also Figure S1 and S4. (**J**) Volcano plot showing differential expression (RNASeq) of 3D7 or $3D7^{MEED}$ both containing the same SLI modification to express PF3D7_0425800. Selected hits were colour coded as indicated. "Exported" refers to all proteins that are known or predicted to be exported but do not fall into the selected families of exported proteins labelled with other colours. Short names are given for colour coded hits when available (full names, accession and total data in Table S3).

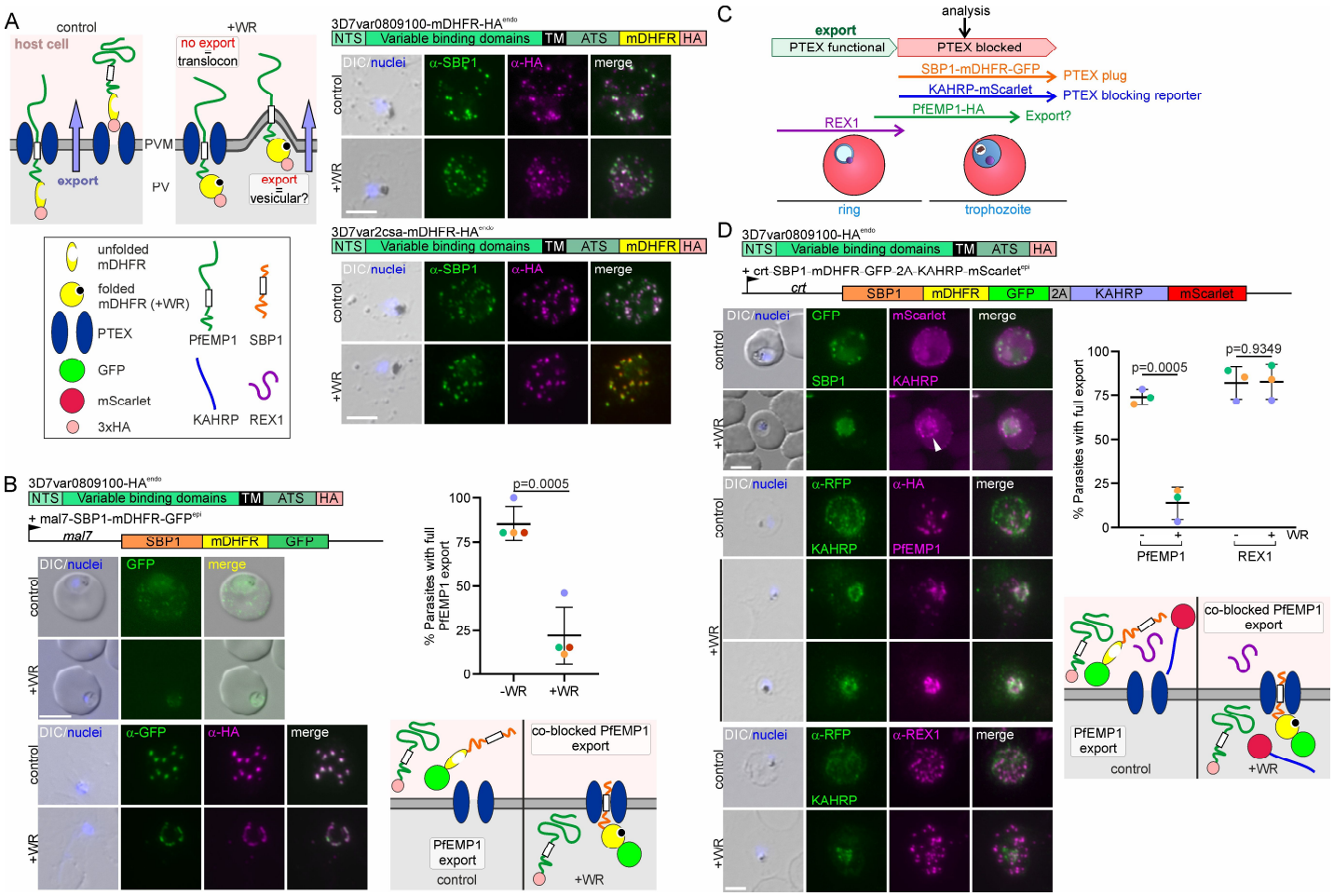

Figure 2. Clogging PTEX prevents PfEMP1 transfer into the host cell. (A) Scheme: options for impact of WR-induced stabilisation of mDHFR folding on PfEMP1 export. Relevant domains of modified PfEMP1 indicated. Fluorescence microscopy images of IFAs with parasites of the indicated cell line + and – WR with the indicated antibodies. Nuclei: Hoechst 33342; DIC: differential interference contrast; size bars 5 µm. (**B**) Effect of blocking PTEX (+WR) with early (*mal7* promoter) expressed SBP1-mDHFR-GFP on PfEMP1 export. Relevant expressed products are shown. Live cell images (top rows) and IFAs (bottom rows; as described in (A)) of parasites grown + and - WR. Graph: quantification of parasites with a PfEMP1 export phenotype + and - WR (4 biological replicates; dots: % cells per replicate; bars: mean of replicates with SD; n = 26 parasites per experiment and condition; +WR only parasites with an SBP1-mDHFR-GFP export phenotype were scored; unpaired t-test; p-values indicated). Scheme shows WR-dependent clogging of PTEX (right) or control (left); features explained in (A). (**C**) Effect of blocking PTEX with late (*crt* promoter) expressed SBP1-mDHFR-GFP-2A-KAHRP-mScarlet on PfEMP1 export. Relevant expressed products are shown. Live cell images (top rows) and IFAs (bottom rows, as described in (A)) + and - WR. Graph: quantification of parasites with PfEMP1 or REX1 export phenotype + and - WR (3 biological replicates; -WR, PfEMP1: n = 34, 76, 60; +WR, PfEMP1: n = 18, 48, 30; -WR, REX1: n = 18, 27, 35; +WR, REX1: n = 12, 31, 25; +WR, only parasites with an KAHRP-mScarlet (late PTEX block reporter) export phenotype were scored (dots: % cells per replicate; bars: mean of replicates with SD; unpaired t-test; p-values indicated). Scheme shows WR-dependent clogging of PTEX (right) or control (left); features explained in (A); note that due to late block, early expressed REX1 is in the host cell in both conditions. See also Figure S2.

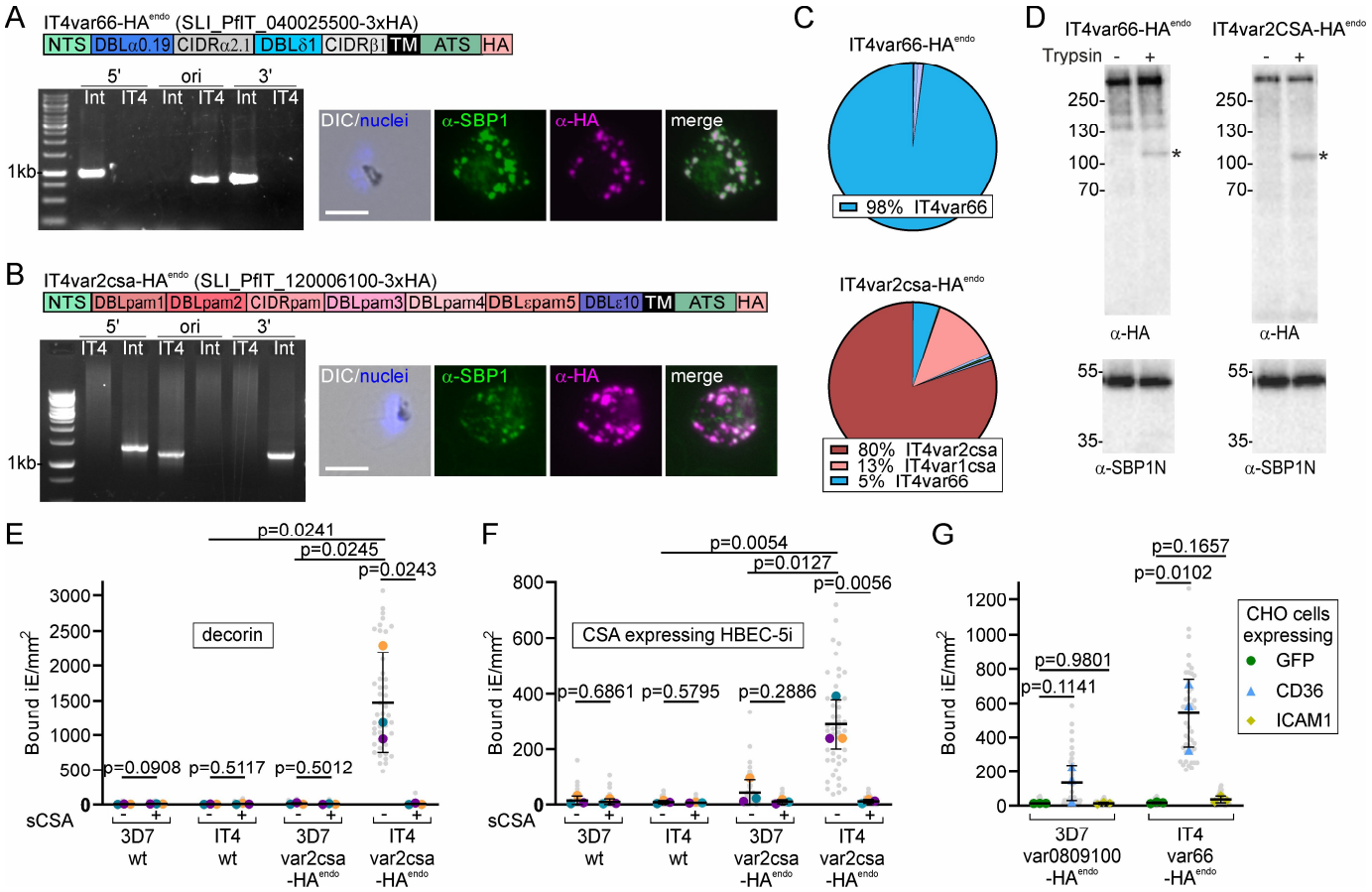

Figure 3. Activated PfEMP1s in IT4 are functional and cytoadherent. (**A**, **B**) Activation of indicated PfEMP1. Scheme shows domain organisation. Agarose gel shows PCR products confirming correct integration of the SLI plasmid as described in Fig. 1A, see Table S6 for sequence of primers used; IT4: parent; Int: integrant cell line. Fluorescence microscopy images show IFAs with indicated antibodies. Nuclei: Hoechst 33342; DIC: differential interference contrast; size bars 5 µm. (**C**) Pie charts show proportions of total *var* gene transcripts of the indicated cell lines determined by RNAseq (normalized to TPM). (**D**) Western blot of trypsin cleavage assays with indicated parasites. Asterisks show protected PfEMP1 fragment. α-SBP1-N: control for integrity of host. Marker in kDa. Replicates and full blots in Figure S4. (**E**, **F**) SuperPlots showing binding assays of indicated cell lines against decorin or CSA-expressing HBEC-5i cells (3 biological replicates with 15 fields of view/experiment and condition; bars: mean of averages of replicates with SD; unpaired t-test; p-values are indicated). Small grey dots: bound iE/field of view, extrapolated to mm^2. Larger coloured dots: average of bound iE/mm^2/replicate. Same colour indicates experiment conducted in parallel. iE: infected erythrocytes. (**G**) SuperPlot of binding assays of indicated cell lines against CHO cells expressing GFP, CD36 or ICAM-1 (3 biological replicates with 15 field of views/ experiment and condition; bars: mean of averages of replicates with SD; unpaired t-test; p-values are indicated). Small grey dots: bound iE/field of view, extrapolated to mm^2. Larger coloured dots: average bound iE/mm^2/replicate. iE: infected erythrocytes.

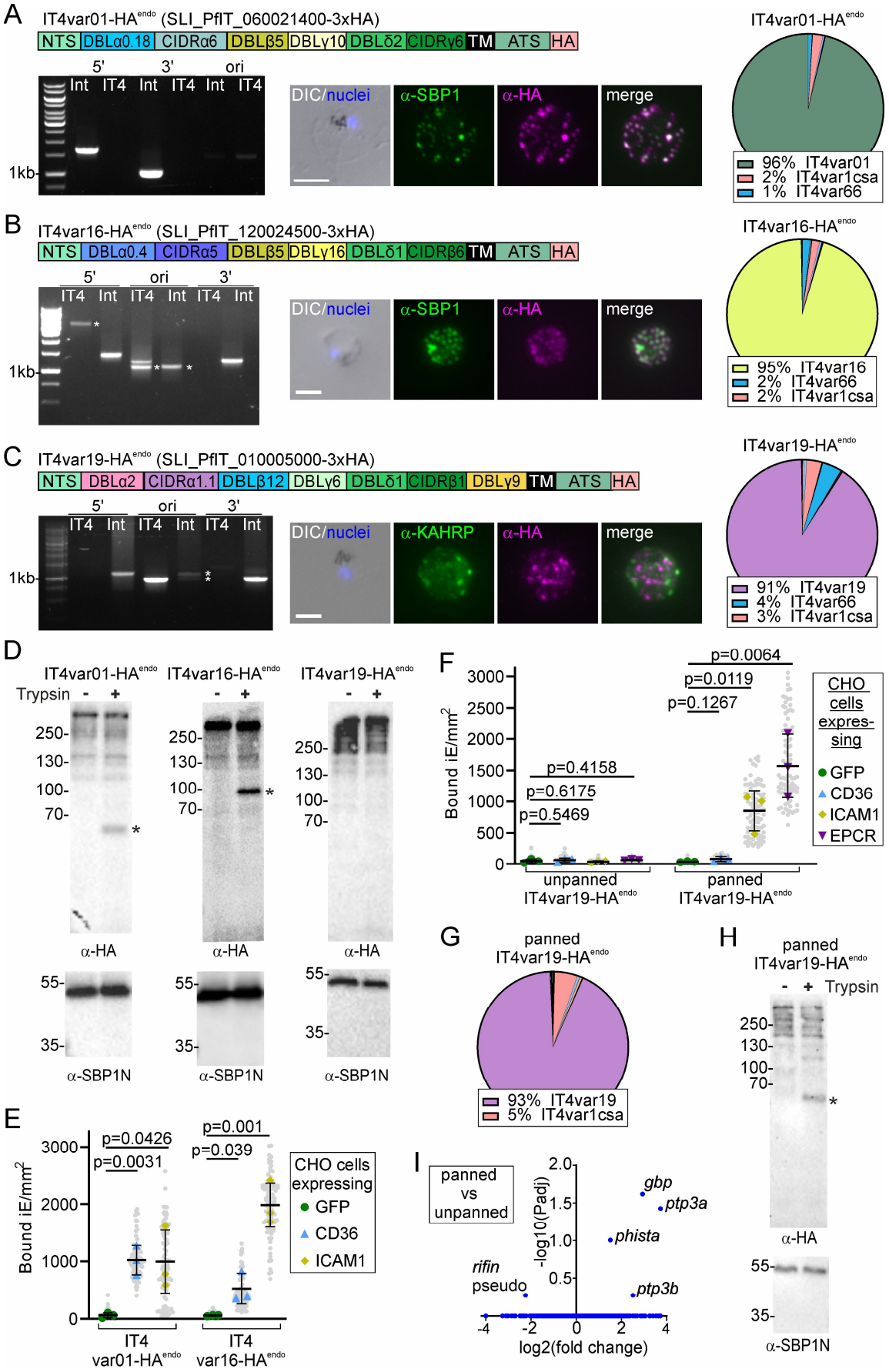

Figure 4. Activation of further PfEMP1s with different binding properties in IT4. (**A**, **B**, **C**) Activation of indicated PfEMP1. Scheme shows domain organisation. Agarose gel shows PCR products confirming correct integration of the SLI plasmid as described in Fig. 1A, see Table S6 for sequence of primers used; IT4: parent; Int: integrant cell line. Asterisks

indicate non-specific bands; for the original locus this likely includes bands from other *var* genes that result in PCR products of slightly different size to that of the correct *var* gene. Fluorescence microscopy images show IFAs with indicated antibodies. Nuclei: Hoechst 33342; DIC: differential interference contrast; size bars 5 µm. Pie charts show proportions of total *var* gene transcripts of the indicated cell lines determined by RNAseq (normalized to TPM). (**D**) Western blot of trypsin cleavage assays with indicated parasites. Asterisks show protected PfEMP1 fragment. α-SBP1-N: control for integrity of host cell. Marker in kDa. Replicates and full blots in Figure S4. (**E, F**) SuperPlots of binding assays of indicated cell lines against CHO cells expressing GFP, CD36, ICAM-1 or EPCR (3 biological replicates with 15 fields of view/experiment and condition; bars: mean of averages of replicates with SD; unpaired t-test; p-values are indicated). Small grey dots: bound iE/field of view, extrapolated to mm^2. Larger coloured dots: average of bound iE/mm^2/replicate. iE: infected erythrocytes. (**G, H**) Pie chart showing proportions of total *var* gene transcripts as determined by RNAseq (normalized to TPM) and Western blot of trypsin cleavage assay as described in (D) of IT4var19-HA^{endo} parasites after five rounds of panning on EPCR. See also Figure S1. (I) Volcano plot showing differential expression analysis (DeSeq2) of EPCR-panned against unpanned IT4var19-HA^{endo} parasites.

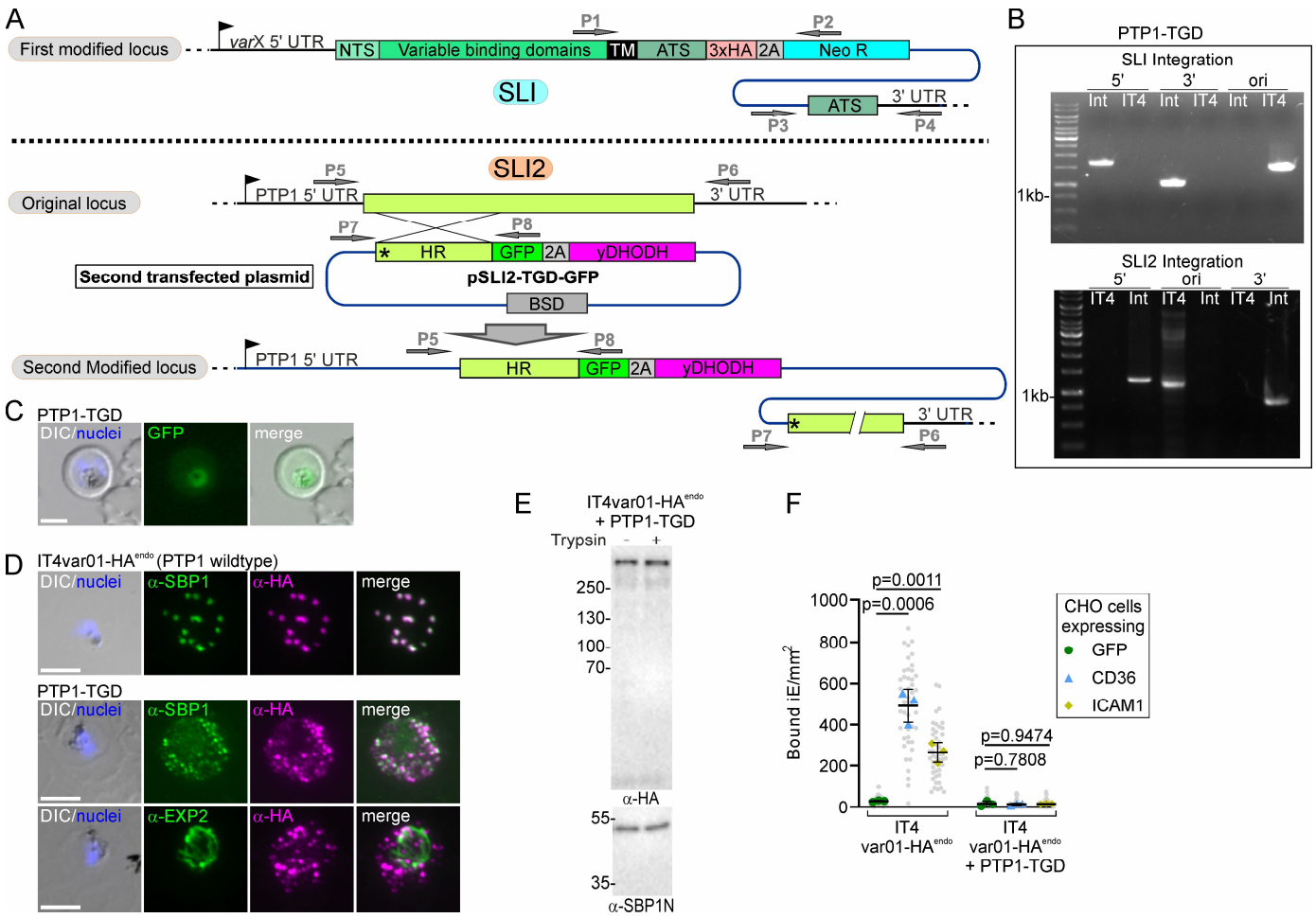

Figure 5. Second endogenous modification with SLI2 in a SLI *var* gene cell line. (**A**) Schematic for SLI2 strategy for second genome modification in SLI cell line with activated *var* gene. HR: homology region; ATS: acidic terminal segment; NTS: NTS domain; 2A: T2A skip peptide; NEO-R: neomycin-resistance gene; yDHODH: yeast dihydroorotate dehydrogenase; BSD: Blasticidin-S-deaminase gene, arrows P1-8 primers for diagnostic PCR; X: desired *var* gene; PTP1: PfEMP1 transport protein 1. (**B**) Agarose gel shows PCR products confirming correct integration of the SLI2 plasmid and perpetuation of the SLI plasmid integration. SLI2 integration: product over 5′ integration junction (5'): P5 + P8; over 3' integration junction (3'): P7 + P6; original locus (ori): P5 + P6; SLI integration PCRs as described in Fig. 1A; IT4: parent; Int: integrant cell line; primers in Table S6. (**C**) Fluorescence microscopy images of live IT4var1-HA^{endo}+PTP1TGD-GFP parasites. (**D**) Fluorescence microscopy images of IFAs with indicated antibodies. Nuclei: Hoechst 33342; DIC: differential interference contrast; size bars 5 µm. Nuclei: Hoechst 33342; DIC: differential interference contrast; size bars 5 µm. (**E**) Western blot of trypsin cleavage assays with IT4var1-HA^{endo}+PTP1-TGD parasites. α-SBP1-N: control for integrity of host cell. Marker in kDa. Replicates and full blots in Figure S4. (**F**) SuperPlot of binding assays of indicated cell lines against CHO cells expressing GFP, CD36 or ICAM-1 (3 biological replicates with 15 fields of view/experiment and condition; bars: mean of averages of replicates with SD; unpaired t-test; p-values are indicated). Small grey dots: bound iE/field of view, extrapolated to mm^2. Larger coloured dots: average of bound iE/mm^2/replicate. iE: infected erythrocytes.

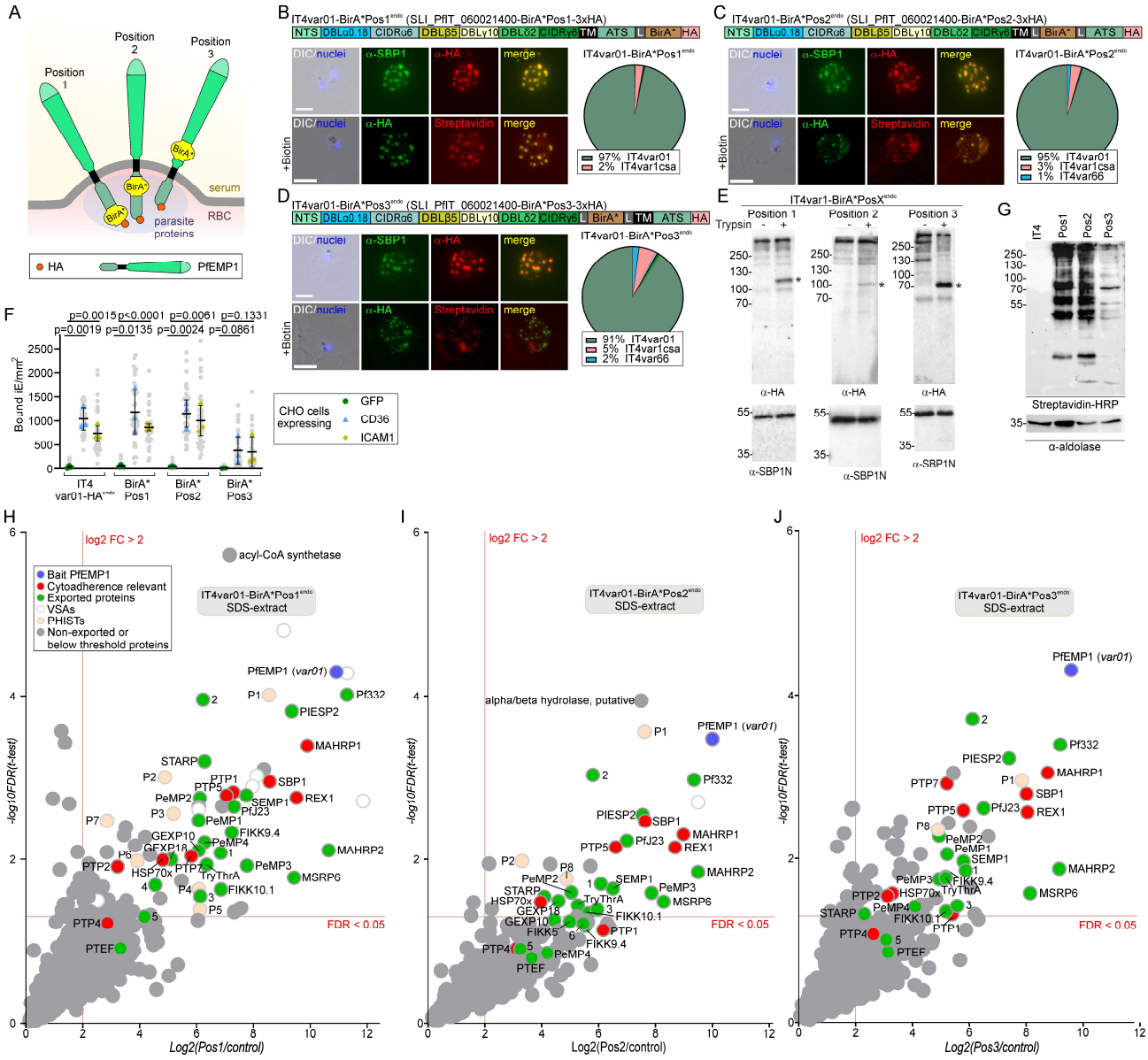

Figure 6. Proxiome of PfEMP1 from living parasites. (**A**) Schematic of the three different 3xHA-tagged BirA*-IT4var1 fusion constructs and the position respective to the membrane in the fusion constructs reaching the host cell surface. (**B**, **C**, **D**) Confirmation of the activation and modification of the indicated IT4var1-BirA* fusions. Fluorescence microscopy images show IFAs with indicated antibodies or streptavidin. Nuclei: Hoechst 33342; DIC: differential interference contrast; size bars 5 µm. Pie charts show proportions of total *var* gene transcripts of the indicated cell lines determined by RNAseq (normalized to TPM). (**E**) Western blot of trypsin cleavage assays with indicated parasites. Asterisks show protected PfEMP1 fragment. α-SBP1-N: control for integrity of host cell. Marker in kDa. Replicates and full blots in Figure S4. (**F**) SuperPlot of binding assays of indicated cell lines against CHO cells expressing GFP, CD36 or ICAM-1 (3 biological replicates with 15 fields of view/experiment and condition; bars: mean of averages of replicates with SD; unpaired t-test; p-values are indicated). Small grey dots: bound iE/field of view, extrapolated to mm^2. Larger coloured dots: average of bound iE/mm^2/replicate. iE: infected erythrocytes. (**G**) Western blot of extracts of the indicated cell lines after incubation with biotin for 24 hours. Streptavidin probes biotinylated proteins; α-aldolase is the loading control. (**H**, **I**, **J**) Volcano plots showing enrichment of biotinylated proteins extracted with SDS from the indicated cell lines compared to IT4 wildtype parasites (24 hours growth with biotin) (full data in Table S4). Only the quadrant with positive enrichment is shown, full plots in Figure S5 and further comparisons in Figure S6. Hits are colour coded as indicated and short names are given in the plot for known proteins. Phists and other exported proteins without short name were numbered (accessions are found under abbreviations in Table S4).

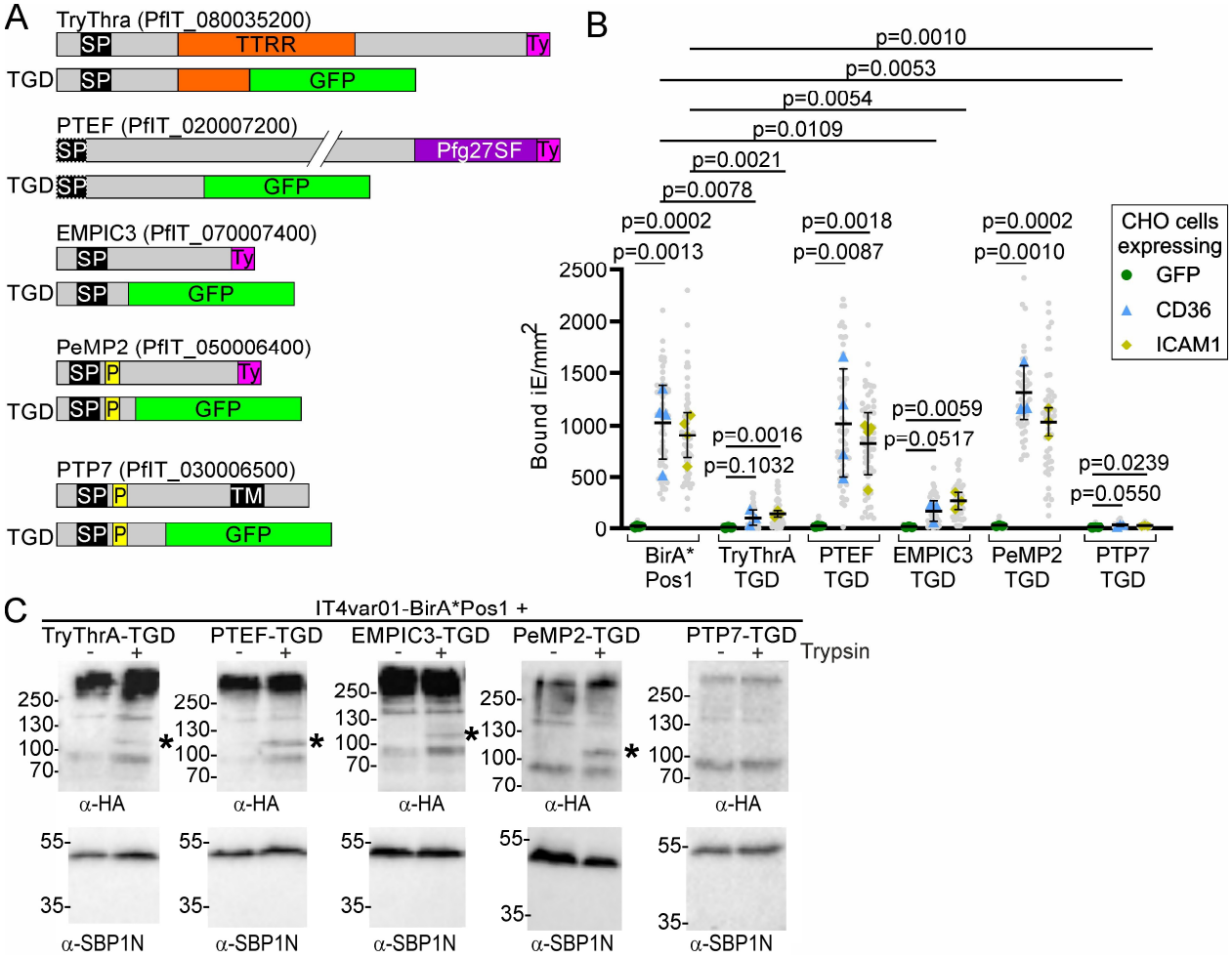

Figure 7. New proteins needed for PfEMP1 cytoadherence function. (**A**) Domain schematic of candidates selected for analysis (Ty1-tagging and disruption (TGD) using SLI2) in IT4var1-BirA*Pos1^{endo}. (**B**) SuperPlot of binding assays of the indicated cell lines against CHO cells expressing GFP, CD36 or ICAM-1 (3 or 4 (control and PTEF-TGD) biological replicates with 15 fields of view/experiment and condition; bars: mean of averages of replicates with SD; unpaired t-test; p-values are indicated). Small grey dots: bound iE/field of view, extrapolated to mm^2. Larger coloured dots: average of bound iE/mm^2/replicate. iE: infected erythrocytes. (**C**) Western blot of trypsin cleavage assays with indicated parasites. Asterisks show protected PfEMP1 fragment. α-SBP1-N: control for integrity of host cell. Marker in kDa. Replicates and full blots in Figure S4. See also Figure S7 and S8.